applied sciences

MDPI

Article

ROAD Statistics-Based Noise Detection for DME Mitigation in LDACS

Miziya Keshkar [1], Raja Muthalagu [2,*] and Abdul Rajak [1]

[1] Department of Electrical and Electronics Engineering, Birla Institute of Technology and Science Dubai Campus, Dubai 345055, United Arab Emirates; miziyak@gmail.com (M.K.); abdulrazak@dubai.bits-pilani.ac.in (A.R.)
[2] Department of Computer Science, Birla Institute of Technology and Science Dubai Campus, Dubai 345055, United Arab Emirates
* Correspondence: raja.m@dubai.bits-pilani.ac.in

Abstract: Interference mitigation in L-band Digital Aeronautic Communication Systems (LDACS) from legacy users is extremely important as any error in data retrieval of aeronautic communication can adversely affect flight safety. This paper proposes an LDACS receiver prototype which uses rank-ordered absolute differences (ROAD) statistics to detect the distance measuring equipment (DME) interference. The detected DME interference is reduced in the next stage by pulse blanking. The performance of the proposed ROAD pulse blanking method (ROAD PB) is compared with the existing interference mitigation methods which use the amplitude of the received signal for the detection of DME interference. In depth analysis of the obtained results affirms that the proposed ROAD value-based interference detection excels amplitude-based detection. For an SNR value of 0 dB, the proposed method of detection could achieve a 3% increase in terms of accuracy with a reduction of 4% in false alarms. With the advantage of ROAD statistics detection, the proposed ROAD PB could achieve an SNR saving of 2.7, 1.1, 0.7, 0.25 and 0.2 dBs at BER 10^{-1} in comparison with pulse blanking, Genie-aided estimation enhanced pulse peak attenuator (GAEPPA), GAE enhanced pulse peak limiter (GAEPPL), optimum Bayesien estimator enhanced pulse peak attenuator (OBEPPA) and OBE enhanced pulse peak limiter (OBEPPL). The comparative results show that the proposed ROAD pulse blanking outperformed the other techniques for the optimum threshold value of the operation.

Keywords: OFDM; LDACS; aeronautical communication; impulse noise; pulse blanking; ROAD statistics

check for updates

Citation: Keshkar, M.; Muthalagu, R.; Rajak, A. ROAD Statistics-Based Noise Detection for DME Mitigation in LDACS. *Appl. Sci.* **2022**, *12*, 3774. https://doi.org/10.3390/app12083774

Academic Editors: Giovanni Randazzo, Dimitrios S. Paraforos, Stefania Lanza and Anselme Muzirafuti

Received: 17 January 2022
Accepted: 1 April 2022
Published: 8 April 2022

1. Introduction

Air traffic growth is happening at a very rapid rate. As per Eurocontrol's latest study report about European aviation in 2040, the air traffic growth will be limited by the available capacity at the airports. This can lead to a rapid increase in congestion at the airport, which in turn can cause extra pressure on the network and more delays [1]. To accommodate this huge increase in air traffic, an efficient air traffic management system (ATM) supported by a secure and spectrum-efficient Communications, Navigation and Surveillance (CNS) framework is needed.

The existing air traffic management system is supported by voice and data communications systems. The main voice communication media for air to ground communication is still analog. The existing analog VHF double sideband amplitude modulation (DSB-AM) will remain in service for many more years as it ensures safe and reliable communication with the use of low-cost communication equipment. However, this technology becomes a hindrance in deploying new ATM applications, such as flight centric operation with point-to-point communications [2].

Similar to voice communication, data communication to the cockpit is also ensured by ground-based equipment operating within HF or VHF radio bands. The communication is through narrowband radio channels, which limits the data throughput to some kilobits

per second. These data links are insufficient to provide broadband services now or in the future with the existing VHF and HF spectrum [2]. Hence, the International Civil Aviation Organization (ICAO) has recommended Future Communications Infrastructure (FCI) to modernize the existing communication links with new spectrum-efficient and reliable infrastructure, which can support new ATM applications and broadband services. This led to the development of the L-band (960–1164 MHz) Digital Aeronautical Communication Systems (LDACS) [3].

In 2009, the specification of LDACS was proposed. ICAO suggested two possible standards: LDACS1 derived from the IEEE 802.16 wireless system [3] and LDACS2 derived from the global system for mobile communication (GSM) [4]. LDACS1 uses advanced network protocols of current commercial standards. It is a broadband multicarrier system based on orthogonal frequency division multiplexing (OFDM). LDACS2 uses protocols that offer high QoS communications. It is a narrow band single carrier system based on Gaussian minimum shift keying modulation (GMSK). It is expected to accommodate the huge increase in air traffic with the deployment of any of these subsystems of LDACS.

As shown in Figure 1, L-band is already providing services to legacy users such as distance measuring equipment (DME), military tactical air navigation (TACAN) system and joint tactical information distribution system (JTIDS), which are used for navigation aids. Apart from these, universal access transceiver (UAT) at 978 MHz and secondary surveillance radar (SSR) and airborne collision avoidance system at 1030 and 1090 MHz are also allotted with fixed channels [5–8]. However, studies about spectrum occupancy revealed that large portions of the L-band spectrum are used less frequently or underutilized [3,4]. Hence, the LDACS system is deployed in the L-band either as an inlay system between the legacy users or as an overlay system in the unoccupied spectrum [9]. The overlay method is selected for LDACS2 (960–975 MHz). Though the method is less complex, spectrum scarcity is a noticeable challenge [10–12]. The inlay approach, chosen in LDACS1, is expected to overcome the challenge of spectrum scarcity by utilizing the 1 MHz spectral gap between legacy user DME, thereby increasing the spectrum utilization.

The comparative studies between LDACS1 and LDACS2 affirmed that LDACS1 is the preferred choice over LDACS2. LDACS1 is highly capable of supporting high-speed delay-sensitive multimedia services and is also compatible with the cellular communication standards. LDACS1 is further referred to as LDACS [13,14]. Hence, the work presented in this paper uses LDACS to refer to LDACS1 hereafter.

LDACS involves two way communication: a forward link (FL) from the ground station (GS) to air station (AS) and a reverse link (RL) from AS to GS. It provides frequency division duplexing (FDD) of 63 MHz spacing between FL (962–1213 MHz) and RL (1025–1150 MHz) with the opportunistic access of paired spectrum. The deployment of LDACS in L-band gives rise to interferences to license users and vice versa. The possible interference scenario for LDACS is portrayed in Figure 2. In words, it can be affirmed as follows: (a) LDACS FL is impaired by DME GS (FL), not by DME airborne station (AS), as (RL) is not active in this part of spectrum, (b) LDACS RL is impaired by both the DME GS (FL) and DME AS (RL), (c) DME FL is impaired by interference from both the LDACS GS (FL) and LDACS AS (RL) and (d) DME RL is impaired with interference from LDACS AS (RL), not from LDACS GS (FL), as it is not active in this part of the spectrum.

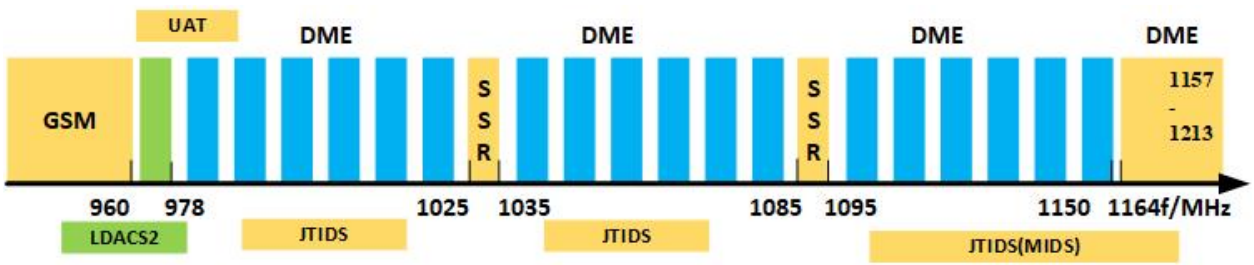

Figure 1. L-band Spectrum Occupancy [9].

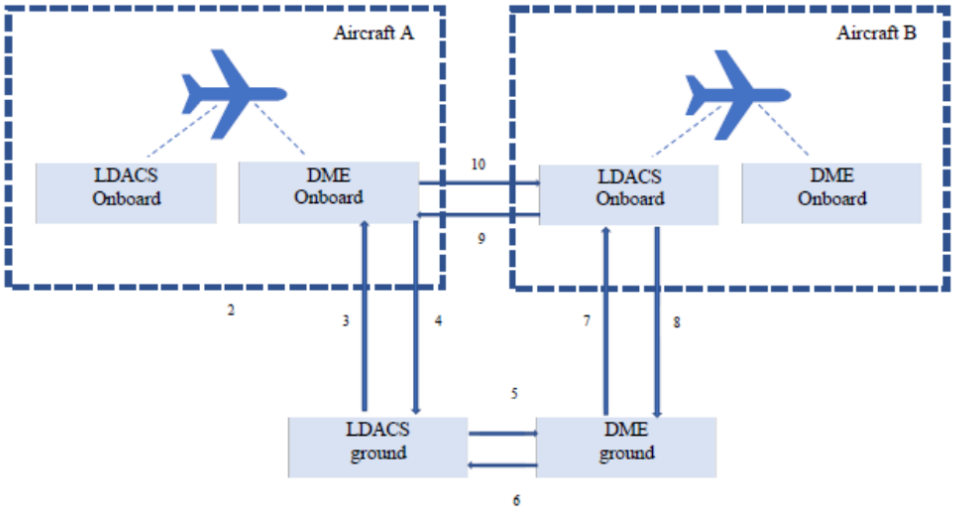

Figure 2. Interference Between DME and LDACS [15].

Identifying the possible interference scenario, the role of interference mitigation is recognized as critically important as any malfunctioning of the licensed system can affect flight safety. The rest of the paper is oriented as follows: Section 2 lists the literature survey of existing DME interference mitigation techniques in LDACS with their advantages and drawbacks. Section 3 expounds on the system and noise model used for this work. Section 4 elaborates the theory and functioning of the proposed method in spotting and reducing DME interference. The section also includes the detailing of nonlinear methods used for the comparison of the proposed method in DME mitigation. Section 5 elucidates the results obtained for the proposed method in terms of reducing the bit error rate in received data with other DME interference reduction techniques. The following are the list of abbreviations used in this paper.

2. Related Work

Several interference mitigation techniques for LDACS are available in the literature; among these, most of the proposed schemes focus on mitigating DME interference. In 2011, two methods capable of detecting and mitigating DME interference were put forward. The monotonous structure and spectral shape of the DME pulse are exploited in proposing these two methods. The methods achieve the merit of simpleness at the cost of losing a portion of data resulting from pulse blanking [16]. In 2012, Hailiang Wang et al. put forward a concoction of pulse blanking and notch filter to reduce the interference. Though the method gives leeway in the time and frequency domain of operation, it is more safe and effective for the B2 band (1900 MHz) signal [17]. Further, Yun Bai et al. proposed a DME mitigation scheme that advantages complementary code keying (CCK). Though the CCK encoding has the merit of better gain, it requires low phase distortion and a wideband channel. The latency of the system is high due to the large acquisition time. Moreover, the modulation employed here is not a power-efficient modulation [18].

In 2014, Q. Li et al. proposed an iterative receiver design [19]. The design employs iterative decoding between the demodulator and decoder based on the Turbo principle. Another type of selective pulse blanking method to curtail DME interference is put forward in [20]. The method bestowed a designed fast filter bank for this purpose. In 2016, Li Douzheetal et al. propounded a method based on deformed pulse pair spotting and its subtraction from the actual signal [21]. Later, Khodr A. Saaifan and Werner Henkel insinuated lattice signal sets to resist DME interference. Precoding based on lattice signal set at the transmitter changes the shape of the DME signal spectrum. A simple clipping technique is then applied for DME mitigation [22].

The major flaw of pulse blanking is recognized as intercarrier interference. In [9], decision-directed noise estimation is put forward to eliminate the intercarrier interference.

Reduced throughput of transmission and wastage of power are the drawbacks of this scheme. LDACS-OFDM based on discrete wavelet transform (DWT) is discussed in [23]. The scheme makes use of the real nature of DME. The signal affected with DME is selectively transmitted through the quadrature channel. With the effective utilization of direct sequence spread spectrum to combine the in phase and quadrature phase, the method proclaims the elimination of DME. The computational complexity and resource requirement are the flaws present in this scheme. In [24], an energy-based DME detector has been proposed. The detector works with adaptive threshold value in order to obtain the best trade-off between DME signal detection and false alarm. In 2021, a deep clipping-based DME noise reduction technique is propounded in [25]. It is a linear clipping method that uses two threshold levels for recognition and reduction in DME. Detailed study of the existing interference mitigation techniques in LDACS exposes active research is going on in this area.

The Genie-aided estimator (GAE) taps the statistical description of the side information to generate the design parameters to accomplish lower bounds on the bit error at the receiver [26]. However, details of the side information are required to accomplish this lower bound performance. The correlation of the impulsive noise or the frequency in impulsive noise arrival time is some other side information [27]. When a Gaussian source is influenced by uncorrelated impulse noise, it is possible to attain optimum system performance with the use of a Bayesian signal estimator. In 2013, P. Banelli proposed an optimal Bayesian estimator (OBE) mainly for real-valued Gaussian mixture noise [28]. Later, the method was further upgraded for complex signals in 2015 [29]. It is possible to propose different types of pulse peak attenuators and pulse peak limiters for DME mitigation with the estimation knowledge obtained from GAE and OBE [30]. In this paper, we have used GAE and OBE enhanced pulse peak attenuators and limiters to compare the performance of the proposed ROAD pulse blanking.

ROAD statistics-based impulse detector was proposed in 2005 to detect the impulse pixels in an image. The idea can be extended to remove any mix of Gaussian and impulse noise [31]. In [32], the ROAD value of the received signal is used as one of the inputs to train the deep neural network for the detection of signal instances corrupted with impulse noise. The most affected or least acceptable data are present on those subcarriers whose powers are much different from neighboring subcarriers at each time epoch. Hence, it is possible to use ROAD statistics to identify the subcarriers affected with impulse noise. To the best of our knowledge, no work has been reported that employs ROAD statistics for the detection of DME interference to date.

In this paper, ROAD pulse blanking is proposed which uses ROAD statistics for the detection of DME interference and pulse blanking for noise mitigation. The performance of the proposed method is compared with absolute value-based DME interference detection methods such as pulse blanking, GAE enhanced pulse peak attenuators/limiters and OBE enhanced pulse peak attenuators/limiters.

All these methods include two basic operations:

1. Detection of DME interference.
2. Mitigation of DME interference.

The advantage of the proposed method compared to other methods is that it could identify affected subcarriers more accurately and hence could eliminate noise more effectively. The performance of pulse blanking is observed to be improved when ROAD statistics-based noise detection has been employed. The improvement in performance is such that it outperformed GAE enhanced pulse peak attenuators/limiters and could stand with OBE enhanced pulse peak attenuator/limiter.

3. System and Noise Model

LDACS System Model

The system model includes the LDACS transmitter, the channel which imparts additive white Gaussian (AWGN) noise and DME interference and the LDACS receiver. Figure 3

elaborates the detailed block diagram of the LDACS ground station transmitter. Data source creates random data of 91 bytes and passes to Reed–Solomon (RS) coder resulting in an extra 10 bytes of redundant data for error correction and detection. A 6-bit zero padding is performed on the output of the RS coder before passing to the convolutional coder. The coded output of the convolutional coder is made to pass through permutation interleaver for reducing burst errors. The output of permutation interleaver is arranged into a standard LDACS data format (F) after symbol mapping, modulating with Quadrature Phase Shift Keying (QPSK) and frame composing. All the variables shown in Figures 3 and 4 are generated for standard LDACS data frame format (F). The same variables with suffix 't' signify the same signal for an instant 't' or the tth OFDM symbol. In other words, $F_t = [F_t[0], F_t[1]...F_t[N-1]]^T$ stands for the tth symbol of LDACS forward link frame (F) with N orthogonal subcarriers. F_t carries the random data $F_t[m]_{m=0,1...N-1}$ with zero mean and variance σ_F^2. The OFDM symbol $S_t = [S_t(0), S_t(1)...S_t(N-1)]^T$ is generated in the time domain by calculating the 64-point IFFT of the data F_t. Further, N_{CP} number of cyclic prefix bits are added to the total N subcarriers resulting in transmitted vector $X'_t = \left[X'_t(0), X'_t(1)\ldots, X'_t\left(N+N_{cp}-1\right)\right]$.

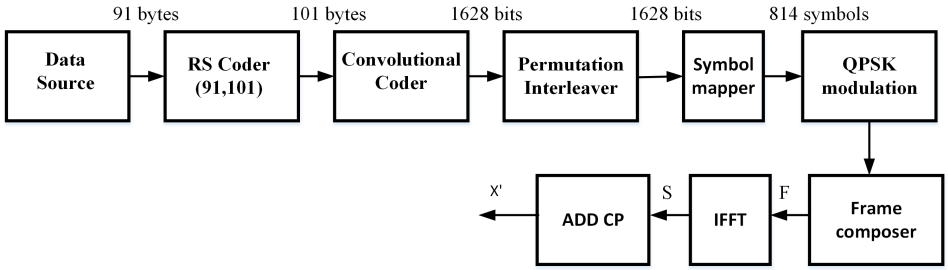

Figure 3. LDACS transmitter block diagram.

The transmitted signal X' changes to r' when it passes through the channel in the presence of DME. For each instant t, the transmitted vector X'_t is affected by a noise component $i_t = [i_t(0), i_t(1), ..., i_t(N+N_{cp-1})]^T$ which is a mixture of the additive white Gaussian noise $A_t = [A_t(0), A_t(1), ..., A_t(N+N_{cp-1})]^T$ and the impulse noise (DME) $p_t = [p_t(0), p_t(1), ..., p_t(N+N_{cp-1})]^T$. Thus, the received signal for an instant 't' is $r'_t = \left[r'_t(0), r'_t(1), r'_t\left(N+N_{cp}-1\right)\right]^T$ and can be denoted as in (1).

$$r'_t = X'_t + i_t \tag{1}$$

where

$$i_t = A_t + p_t \tag{2}$$

As discussed in Section 1, the prime contributor of interference to LDACS is DME. These signals are a pair of Gaussian-shaped pulses, separated by a duration of Δt. The transmission rate (30 pulse pairs per second or 50 ppps), as well as the duration Δt (12 or 36 µs) of DME signals, varies with the mode of operation of the distance measuring equipment. A pair of DME pulses in the baseband can be expressed as in (3) [33].

$$P_d(t) = e^{\frac{-\zeta t^2}{2}} - e^{\frac{-\zeta(t-\Delta t)^2}{2}} \tag{3}$$

where $\zeta = 4.5 \times 10^{11}$ s^{-2}.

It has a width of 3.5 µs at half of the maximum amplitude. The frequency domain representation of DME signal is as in (4). The spectrum is modulated with a cosine as the pulses are always happening pairwise [34].

$$I_{pd}(f) = \sqrt{\frac{8\pi}{\zeta}} e^{\frac{2\pi^2 t^2}{\zeta}} .e^{-j\pi f \Delta t} cos(\pi f \Delta t) \tag{4}$$

The base band DME pulse pairs are modulated to the relative carrier frequency of the channel to 0.5 MHz left and to 0.5 MHz right of the LDACS system bandwidth. The DME interfering signal that affects the LDACS system is expressed in (5). $I_{pd}(t)$ is the total interference signal for a time interval 't' caused by N number of DME stations that are operating on the 0.5 MHz offset to the center frequency of the LDACS system [35].

$$I_{pd}(t) = \Sigma_{i=0}^{N_{pd}-1}\Sigma_{l=0}^{N_i-1}\sqrt{P_{i,l}}P_d(t-t_{i,l})e^{j2\pi f_{c,i}t+j\chi_{i,l}} \quad (5)$$

where N_{pd} is the total number of interfering DME stations, N_i is the total number of pulse pair in the particular time interval for the ith interfering DME station, $P_{(i,l)}$,$\chi_{(i,l)}$ are power and phase of the pulse pair, respectively, $f_{(c,i)}$—the relative carrier frequency of the ith interfering DME station and $t_{(i,l)}$ is the starting time of the lth pulse pairs of the ith DME station. The methods used to reduce impulse noise work well to reduce DME noise also.

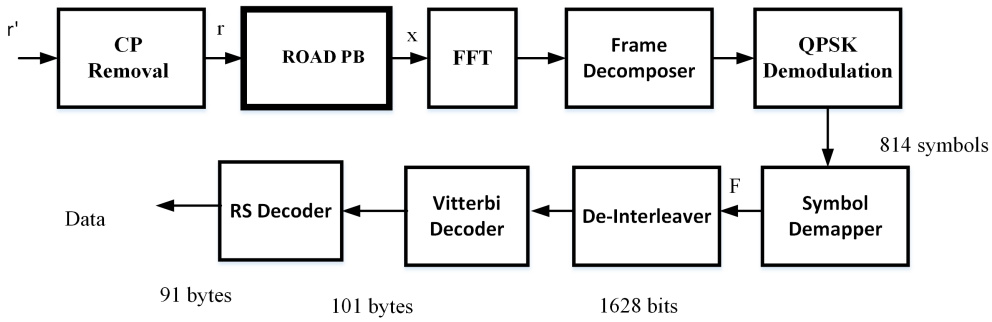

Figure 4. Proposed LDACS receiver block diagram.

The detailed block diagram of the proposed LDACS FL AS receiver is sketched in Figure 4. The first block in receiver removes the cyclic prefix bits associated with the received signal $r' = [r'_t(0), r'_t(1), ..., r'_t(N + N_{C_P-1})]^T$ resulting in signal $r_t = [r_t(0), r_t(1), ... r_t(N-1)]^T$. The nonlinear device ROAD PB detects the DME interference in LDACS signal r (with the clever use of ROAD statistics) and performs pulse blanking to reduce the bit error rate in received data. In general, the resulting vector can be defined as $x = f(r)$ or $x_t = f(r_t)$, where $f(.)$ is the nonlinear function with enough intelligence to sense DME interference. The nonlinear devices discussed in this paper process the signal r_t in dissimilar ways to sense the DME interference. Moreover, the nonlinear estimators used for the performance comparison of the proposed method utilize one more vector π_t to estimate the received signal data. Hence, the definition of function $f(.)$ varies with different nonlinear devices.

The nonlinear device is operated on the signal r before the DFT processing to block the dispersion of sparse time domain impulses $p_t[n]$ over all the OFDM carriers in the frequency domain.

4. Nonlinear Estimators

As discussed in the system model, the nonlinear device is designed to detect and eliminate DME interference from the LDACS AS receiver. In this paper, the proposed nonlinear device ROAD PB uses ROAD statistics for the detection of DME interference and pulse blanking for the mitigation of interference. The performance of the method is compared with the conventional pulse blanking, which uses the amplitude of the received signal for the detection of DME interference. In addition, nonlinear estimators such as GAE enhanced pulse peak processors and OBE enhanced pulse peak processors are also used for the mitigation of DME interference to compare the performance of ROAD PB.

The functioning of the nonlinear devices ROAD PB, pulse blanking, GAEPPA, GAEPPL, OBEPPA and OBEPPL in the detection and elimination of DME noise are discussed below.

4.1. Proposed ROAD PB

When the LDACS signal is affected by DME interference, the amplitude of the received data exhibits a large variation in amplitude from neighboring data. The variation in amplitude due to bit change or additive white Gaussian noise is less due to DME interference. Therefore, the most affected data are those whose amplitude is much different from neighbors. The proposed ROAD PB uses ROAD statistics to quantify the variation in amplitude of particular LDACS (OFDM) data from the neighboring data for each time epoch. Further, the most basic threshold-based detection approach is utilized to identify the data signal affected by DME interference. The goal of fixing a suitable threshold is to recognize the OFDM data that are significant outliers.

The calculation of ROAD value [32] for a one-dimensional LDACS OFDM symbol involves the following steps:

1. The received OFDM symbol for each time epoch is considered as a one-dimensional vector. For a one-dimensional vector of size (1 × 2f + 1), the absolute difference between a center sample and a receiving sample for each time epoch $f_d(k)$ are calculated as in (6)
$$f_d(k) = |r_k - [r_{k-f}, ..., r_{k+f}]| \tag{6}$$
2. The difference vector ($f_d(k)$) is sorted in increasing order.
$$Q(k) = sort(f_d(k)). \tag{7}$$
3. The ROAD value is calculated as the sum of first f values of $Q(k)$
$$ROAD = \Sigma_{k=1}^{f} Q(k). \tag{8}$$

The simple way to recognize the effectiveness of ROAD statistics is to incorporate the method into any existing DME mitigation method. Hence, the proposed ROAD PB incorporates ROAD statistics into pulse blanking. The mathematical depiction of ROAD pulse blanking is as in (9). Here, R_p is the lower threshold value used to discriminate LDACS signals affected with DME interference.

$$x_{|R_P|}(r) = \begin{cases} |r|e^{jarg(r)} & \text{if } ROAD(r) \leq R_p \\ 0 & \text{Otherwise} \end{cases} \tag{9}$$

The reduction in bit error rate at the receiver is compared with normal pulse blanking in Section 5.

The extra computational complexity put forward by ROAD PB compared to conventional pulse blanking is the sum of the computational complexity put forward by the steps involved to calculate ROAD value, as in (6)–(8). As these three steps have no complex multiplication in calculating the ROAD value, it is evident that the extra complex multiplication contributed by ROAD PB is zero. Hence, there is no change in number of complex multiplication compared to LDACS OFDM receiver (without any mitigation) or to pulse blanking. As we have used fast Fourier transform in LDACS OFDM receiver, the total number of complex multiplications involved is $(N/2) \cdot log_2(N)$, where N is the number of subcarriers in OFDM signal [36].

The steps in (6) introduce the extra complex additions $N \cdot (N-1)$ or real number addition $2N \cdot (2N-1)$. Hence, the total number of complex additions of LDACS OFDM receiver with ROAD PB is $N \cdot log_2 N + N \cdot (N-1)$. The number of real-time additions put forward by sorting depends on the type of sorting that is used. For instance, if selective sorting is used, it introduces $\frac{N^2 \cdot (N-1)}{2}$ number of real-time additions. Finally, the number of real value additions introduced by step (8) is $\frac{N \cdot (N-1)}{2}$. The proof is included in Appendix A.

4.2. Conventional Pulse Blanking

The method pulse blanking makes the signal zero if the absolute value of the received signal is above a particular threshold value α_p. The mathematical depiction of pulse blanking is as in (10),

$$x_{|P|}(r) = \begin{cases} |r|e^{jarg(r)} & \text{if } |r| \leq \alpha_p \\ 0 & \text{Otherwise} \end{cases} \tag{10}$$

4.3. Pulse Peak Processors

As discussed in the system model, data estimation needs one more vector π_t along with r_t in performing the nonlinear function $f(\pi_t, y_t)$. The detailing of the nonlinear operations performed by pulse peak attenuators and limiters are depicted in block diagrams Figures 5 and 6, respectively. The received data (after CP removal) r are passed through a 2-GMM estimation block to extract the vector π_t. The parameters contained in vector π_t are further used to compute scaling factor μ_t for each time epoch. From Figure 5, it is clear that pulse peak attenuator uses this parameter μ for processing the signal r_t.

From Figure 6, it is to be noted that pulse peak limiters have one extra block compared to pulse peak attenuators. It is denoted as a decision device that holds the algorithm to change or update the scaling factor. The decision device determines if the scaling factor is needed to modify or not. When the scaling is performed with a modified scaling factor, pulse peak attenuators become pulse peak limiters. In this paper, we have included two types of pulse peak attenuators and four types of pulse peak limiters to compare the performance of proposed ROAD statistics.

It is inevitable to discuss K-GMM modeling to understand the vector π_t in more detail. This section outlines how GAE and OBE enhanced pulse peak processors exploit 2-GMM estimation (2-GMM) to scale the signals affected with DME.

Any random variable can be expressed as the combination of K-number mutually exclusive Gaussian variables with K-GMM modeling [37,38]. Hence, this model can be effectively applied to any ImpN distribution (Class A, S-α-S noises, etc.), either estimated [39–41] and approximated by a K-GMM [42] or modeled with the actual equation [43]. The K-GMM model is mathematically expressed with pdf,

$$f_W(i) = \Sigma_{k=0}^{K-1} P_k \cdot G(i, \sigma_k^2) \tag{11}$$

where $\{P_k\}_{k=0,1,.....K-1}$ with $\Sigma_{k=0}^{K-1} p_k = 0$ are the probability of occurrence of each Gaussian component k. For the value $k = 0$, the component $i_0 \approx G(i_0, \sigma_0^2)$ represents the thermal noise with variance σ_0^2 and with the probability of occurrence p_0 . For values $k = 1$ to $K - 1$, the statistical combinations of components characterize the impulse noise with the probability $p_I = 1 - p_0$ and noise power σ_I^2. The ratio of thermal noise to impulse noise is expressed as $\Gamma = \frac{\sigma_0^2}{\sigma_I^2}$. For the value $K = 2$, this model will reduce to 2-GMM with a thermal noise component $i_0 \approx G(i_0, \sigma_0^2)$ and an impulse noise component $i_1 \approx G(i_1, \sigma_1^2)$.

The 2-GMM model is simple and assumes the presence of a strong impulsive noise as the recognition of only two mutually exclusive events, with probability p_0 and p_1. Hence, 2-GMM is exploited to employ GAE and OBE enhanced pulse peak processors as DME interference mitigators in LDACS receivers. The received signal r, when passed through 2-GMM estimation, results in parameters thermal noise component and impulse noise component with a probability of p_0 and p_1 for each time epoch. Thus, the vector π holds parameters $\sigma_0^2, \sigma_1^2, p_0$ and p_1 obtained from 2-GMM estimation. These parameters are used to calculate the instant scaling parameter μ_t to apply instant nonlinearity to the affected subcarriers in the time domain. The parameter μ varies with different types of pulse peak processors.

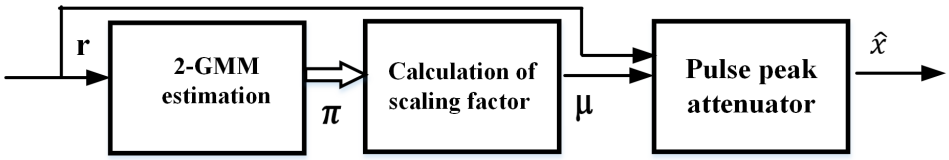

Figure 5. General block diagram for pulse peak attenuator.

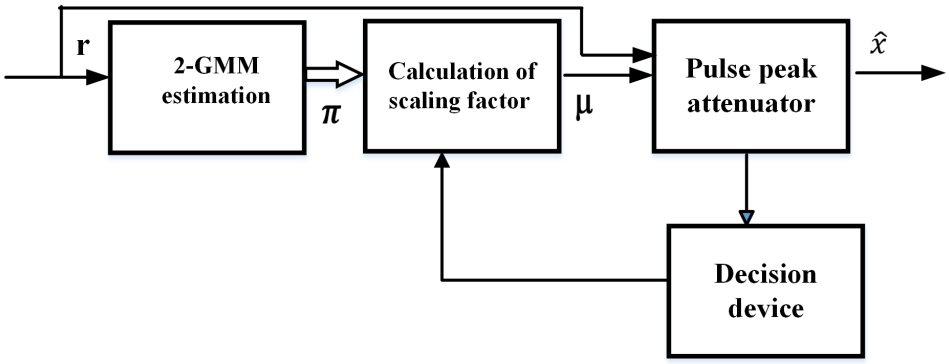

Figure 6. General block diagram for pulse peak limiter.

GAE Enhanced Pulse Peak Processors

The pulse peak processors included in this section are GAE enhanced PPA and GAE enhanced PPLs (Type I and Type II). These pulse peak processors have better performance than GAE by utilizing other side information, such as impulsive noise arrival time or relationship of the impulsive noise [30].

The received signal r can be expressed as the sum of transmitted signal X and noise $i|_k$, where X and $i|_k$ are two zero-mean independent Gaussian random variables with variances σ_X^2 and σ_i^2. With any impulse noise, when modeled as properly weighted mutually exclusive Gaussian events, the GAE claims to know which is the kth Gaussian component of the (pdf), which actually affects the transmitted signal at each time epoch. Once the signal affected with DME interference is identified, all three GAE enhanced pulse peak processors use the same knowledge of GAE for pulse peak processing. The amplitude of the received signal is used for the detection of DME as in pulse blanking.

The GAE enhanced PPA attenuates the nonlinear input r when the amplitude of the received signal exceeds the threshold value. The operation of GAE enhanced PPA can be expressed as follows:

$$\hat{x}_{|kPA|}(r) = \begin{cases} |r| & \text{if } |r| \leq \alpha_p \\ \rho_k \cdot |r| & \text{otherwise.} \end{cases} \tag{12}$$

where $\rho_k = \frac{\sigma_x^2}{\sigma_x^2 + \sigma_k^2}$

$$And, \sigma_k^2 = (1 + \frac{k}{A\Gamma})\sigma_0^2 = \frac{k/A + \Gamma}{1 + \Gamma}\sigma_i^2 = \frac{k}{A\Gamma}\sigma_I^2 + \sigma_0^2 \tag{13}$$

As the device is a pulse peak attenuator, the scaling factor μ is ρ. The scaling factor changes at each instant t as it is a function of r_t and π_t.

GAE enhanced PPA has better performance than the pulse blanking method as it attenuates the DME affected signal rather than losing the data by blanking. The device is well suited to process complex data signals as in LDACS with the modified equation as follows:

$$\hat{x}^*_{|kPA|}(r) = \begin{cases} |r|e^{jarg(y)} & \text{if } |r| \leq \alpha_p \\ \rho_k \cdot |r|e^{jarg(r)} & \text{otherwise.} \end{cases} \tag{14}$$

GAE enhanced PPL is a modified or improved form of GAE enhanced PPA. It employs a decision device to update the scaling factor to attenuate the received signal continuously until the amplitude of the received signal reaches the threshold value (α_p). The repeated attenuation will not affect other subcarriers which are not affected with DME noise. This nonlinear device has better performance at high SNR values compared to the GAE enhanced PPA. The GAE enhanced PPL processes the input signal r and delivers output $\hat{x}_{kPL}(r)$ as stated in (15).

$$\hat{x}_{|kPL|}(r) = \begin{cases} r & \text{if } |r| \leq \alpha_p \\ \rho_{mod} \cdot r & \text{otherwise.} \end{cases} \tag{15}$$

where $\rho_{mod} = \frac{\sigma_x^2}{\sigma_x^2 + N \cdot \sigma_k^2}$.

Here, the value of N varies directly with the difference in power of received signal and threshold peak detection value at each instant. The maximum value of N occurs when the resulting signal holds no values greater than α_p. With this knowledge, the value of N_{max} is as in (16). The algorithm to support this derivation is from [30]

$$N_{max} = \frac{\sigma_x^2(|r|_{max} - \alpha_p)}{\alpha_p \sigma_k^2} \tag{16}$$

Similar to GAE enhanced PPA, GAE enhanced pulse peak limiters also reduce the drawback of the pulse blanking method with less complexity. The same operation can be performed in another way as in (17)

$$\hat{x}_{|kPLs|}(r) = \begin{cases} r & \text{if } |r| \leq \alpha_p \\ M \cdot \rho_k \cdot r & \text{otherwise.} \end{cases} \tag{17}$$

where the maximum value of value of M is derived as in (18) [30]

$$M_{max} = \frac{\alpha_p}{\rho_k \cdot |r|_{max}} \tag{18}$$

From Equations (15) and (17), the updated scaling factors (μ) for GAEPPL Type I and Type II are identified as ρ_{mod} and $M \cdot \rho_k$. Both the methods are applicable to perform scaling of complex valued data with a slight change in Equations (15) and (17) resulting in (19) and (20), respectively.

$$\hat{x}^*_{|kPL|}(r) = \begin{cases} |r|e^{jarg(r)} & \text{if } |r| \leq \alpha_p \\ \rho_{mod} \cdot |r|e^{jarg(r)} & \text{otherwise.} \end{cases} \tag{19}$$

where $\rho_{mod} = \frac{\sigma_x^2}{\sigma_x^2 + N \cdot \sigma_k^2}$.

$$\hat{x}^*_{|kPLs|}(r) = \begin{cases} |r|e^{jarg(r)} & \text{if } |r| \leq \alpha_p \\ M \cdot \rho_k \cdot |r|e^{jarg(r)} & \text{otherwise.} \end{cases} \tag{20}$$

In both cases, the definition for ρ_{mod} and M remains the same as that used in Equations (15) and (17).

4.4. OBE Enhanced Pulse Peak Processors

Bayesian estimators are useful in any Gaussian source affected by any Gaussian-mixture noise [28]. The time domain OFDM signal x can be approximated by Gaussian pdf, $f_X(x) = G(x; \sigma_x^2) = \frac{x^2/2\sigma_X^2}{\sqrt{2}}$. The complex valued received signal $r_t[n]$ at the receiver side has real and imaginary parts $r_{t,R}[n]$ and $r_{t,I}[n]$, respectively. Consider that r represents distinctly either the real or the imaginary part of $r_t[n]$. When the received signal of interest

is modeled or approximated as a Gaussian pdf or K-component pdf, the minimum mean square error Bayesian estimators can be effectively utilized along with the knowledge of the signal x_t. By exploiting the statistical dependency between X and i, it is possible to write $f_{(r|X)}(y) = f_i(r - x)$ and $G(r;\sigma_{rk}^2) = G(r;\sigma_x^2) * G(r;\sigma_k^2)$. Here, $*$ stands for convolution operation. Thus, the received noise power σ_{rk}^2 is the sum of the signal power σ_x^2 and kth Gaussian component noise power σ_k^2

$$\sigma_{rk}^2 = \sigma_r^2 + \sigma_k^2 \tag{21}$$

The OBE enhanced pulse peak processors perform Bayesian estimation only when the received signal is identified as DME affected signal. The pulse peak processors included in this section are OBE enhanced pulse peak attenuator and OBE enhanced pulse peak limiters (Type I and Type II).

The device attenuates the nonlinear input r when the amplitude of the received signal is above α_p . The mathematical expression of OBE enhanced pulse peak attenuator is as in (22).

$$\hat{x}_{|kOPA|}(r) = \begin{cases} |r| & \text{if } |r| \leq \alpha_p \\ \beta_o(r) \cdot r & \text{otherwise.} \end{cases} \tag{22}$$

where

$$\beta_o(r) \cdot r = \frac{\Sigma_{k=0}^{K-1} \rho_k p_k G(r;\sigma_{rk}^2)}{\Sigma_{k=0}^{K-1} p_k G(r;\sigma_{rk}^2)} \tag{23}$$

As the device is a pulse peak attenuator, the scaling factor μ is $\beta_o(r)$. It is possible to use this OBE enhanced PPA for processing complex valued signal as well. The mathematical statement for this operation is as given in (24).

$$\hat{x}_{|kOPA|}(r) = \begin{cases} |r| & \text{if } |r|e^{jarg(r)} \leq \alpha_p \\ \beta_o(r) \cdot |r| \cdot e^{jarg(r)} & \text{otherwise.} \end{cases} \tag{24}$$

OBE enhanced PPL is an altered or upgraded form of OBE enhanced PPL, where it reduces the amplitude of the received signal unceasingly until the amplitude of the DME affected subcarrier reaches the threshold value. As the repeated attenuation is performed only for the subcarriers which exceed the threshold value, it will not disturb the subcarriers which are not affected with DME interference. The OBE enhanced PPL process the input signal r and deliver output $x_{KOPL}(r)$ as stated in (25).

$$\hat{x}_{|kOPL|}(r) = \begin{cases} |r| & \text{if } |r| \leq \alpha_p \\ \beta_{mod}(r) \cdot |r| & \text{otherwise.} \end{cases} \tag{25}$$

where

$$\beta_{mod}(r) = \frac{\alpha_p}{|r|} \tag{26}$$

Here, value of $\beta_{mod}(r)$ is the modified scaling factor μ. The modification can be performed in two ways so that $\beta_{mod}(r)$. $|r|$ becomes equal to α_p.

In one method, P multiples of $\beta_O(r)$ is considered as $\beta_{mod}(r)$. In this situation, the maximum value of P for limiting the output (P_{max}) can be expressed as in (27) [30].

$$P_{max} = \frac{\alpha_p}{\beta_{mod}(r)|r|_{max}} \tag{27}$$

In the second method, the value of the noise power component σ_k^2 is boosted R times so that the output of the nonlinear device is limited to the threshold value α_p. In this case, the modified scaling factor $\beta_{mod}(r)$ can be expressed as in (28) [30].

$$\beta_{mod}(r) = \frac{\Sigma_{k=0}^{K-1} \rho_{mod} p_k G(r; \sigma_{rkmod}^2)}{\Sigma_{k=0}^{K-1} p_k G(r; \sigma_{rkmod}^2)} \tag{28}$$

where $\rho_{mod} = \frac{\sigma_x^2}{\sigma_x^2 + R \cdot \sigma_k^2}$ and $\sigma_{rkmod}^2 = \sigma_x^2 + R \cdot \sigma_k^2$. Both the methods are adaptable to complex valued OFDM data signals as in LDACS. This can be stated mathematically as in (29)

$$\hat{x}^*_{|kOPL|}(r) = \begin{cases} |r| e^{jarg(r)} & \text{if } |r| \leq \alpha_p \\ \beta_{mod}(r) \cdot |r| e^{jarg(r)} & \text{otherwise.} \end{cases} \tag{29}$$

5. Results and Discussions

This section exposes the advantages of ROAD statistics-based sensing over amplitude-based sensing in LDACS FL communication. The results obtained from the detailed analysis of threshold ROAD value-based sensing for different threshold values under different SNR conditions are distinctly presented. The section also discusses the performance of the proposed ROAD statistics-based nonlinear device (ROAD PB) in reducing DME interference when employed in OFDM-based LDACS communication. The discussion is based on the results obtained from the MATLAB simulation of the LDACS forward link communication prototype. The performance of the proposed method is compared with the conventional pulse blanking method which uses the amplitude of the received signal for the detection of DME interference. The nonlinear devices such as GAEPPA, GAEPPL, OBEPPA and OBEPPL are also included to compare the performance of ROAD PB. The mathematical model of the LDACS FL GS transmitter (Figure 3) and LDACS FL AS receiver (Figure 3) are developed as per the standards of the LDACS system for all the inner building blocks.

At the transmitter side, random data of 91 bytes are generated by the data source and given as the input of RS coder (91,101) for external coding. Once external encoding is performed by the RS encoder, 6-bit zero padding is performed before passing through internal encoding by the convolutional encoder (171,133). The encoded bits from the output of convolutional coder, with native coding rate half, are further interleaved (using permutation interleaver) and then mapped to symbols (using symbol mapper). The mapped symbols form complex values when they pass through the QPSK modulation block. The frame composer block forms the LDACS FL data/CC frame with proper insertion of pilot values (158), null values (728) and complex data values (2442) over a total of 3328 subcarriers. Further, the time domain composite waveform of this OFDM frame is generated by passing the frame through the IFFT block of length 64. The effect of the introduction of IFFT (windowing) is canceled by adding 16 cyclic prefix bits. Table 1 holds the OFDM system parameters used in this simulation study.

To analyze the performance degradation of the LDACS FL AS receiver due to DME interference, the AWGN channel is considered. The BER variation of the received signal when passed through the AWGN channel without the influence of DME interference is obtained as shown in Figure 7. For the study of interference on LDACS, DME signals are generated by (3) for a duration Δt of 12 µs as shown in Figure 8. The baseband DME pulse pairs are modulated to the relative carrier frequency of the channel to 0.5 MHz left and to 0.5 MHz right of the LDACS1 system bandwidth. A reduction in performance of the LDACS FL AS receiver can be observed when DME interference is allowed to affect the transmitted data. Figure 7 also shows how the existing simple noise reduction method (pulse blanking) improved the performance of the receiver. The threshold value used for the pulse blanking method is 0.3. Careful analysis of Figure 7 reveals the fact that the pulse blanking technique showed a significant improvement in the performance of the receiver at high SNR powers and a slight decrease at low SNR values. The reason for the reduction in

performance of pulse blanking (at low SNR values) is the false detection caused due to the amplitude-based sensing and the resulting extra loss of data. It is possible to reduce this number of false detections by increasing the threshold value of detection. However, high threshold value can lead to an increase in missed detection and more interference power at the output of the receiver. The false detection caused due to the amplitude-based sensing for an SNR value of 15 dB is visible (sample values between 2500 and 3000) in Figure 9.

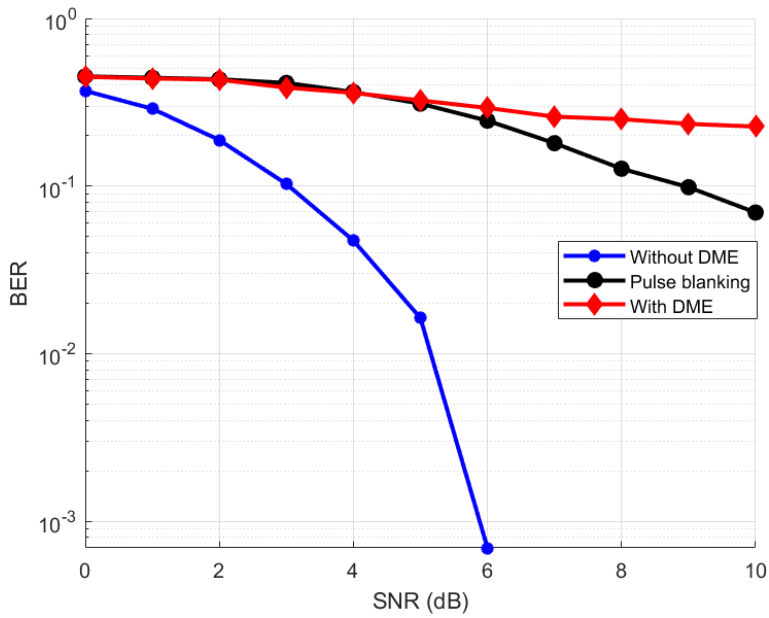

Figure 7. Performance of conventional pulse blanking technique vs. without DME interference and with DME interference.

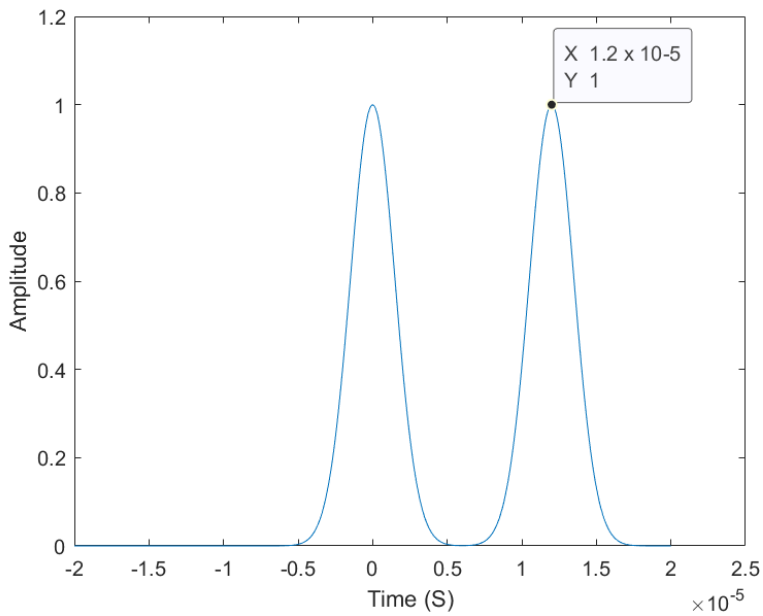

Figure 8. Standard DME pulse pair.

The amplitude of the DME interference signal, amplitude of the received signal along with the threshold value for sensing and the calculated ROAD values of the received signal are plotted in Figure 9. The signals are plotted together to figure out how both amplitude and ROAD value-based sensing accomplishes the detection of DME interference pulses. It can be observed from Figures 9 and 10 that the ROAD values of the received signal is

a magnified (though not exactly) version of absolute difference of each sample from the neighboring sample. Figure 11 depicts how well the ROAD values of the received data could identify the exact location and shape of the DME pulses than amplitude sensing. The performance of both amplitude-based sensing and ROAD statistics-based sensing for a low SNR value (0 dB) is shown in Figure 10. Comparison of Figures 9 and 10 shows that the amplitude-based sensing has less performance for low SNR value 0 dB due to the increased number of false detections. ROAD value-based sensing not only showed improved performance than the other but also preserved it (though not fully) irrespective of the SNR values as the rank-ordered difference value is considered for sensing. It has been observed that the performance of both amplitude-based sensing or ROAD value-based sensing may vary with both the SNR levels and threshold values. Hence, a detailed study of amplitude-based sensing and ROAD value-based sensing have been performed to get more insight of the process.

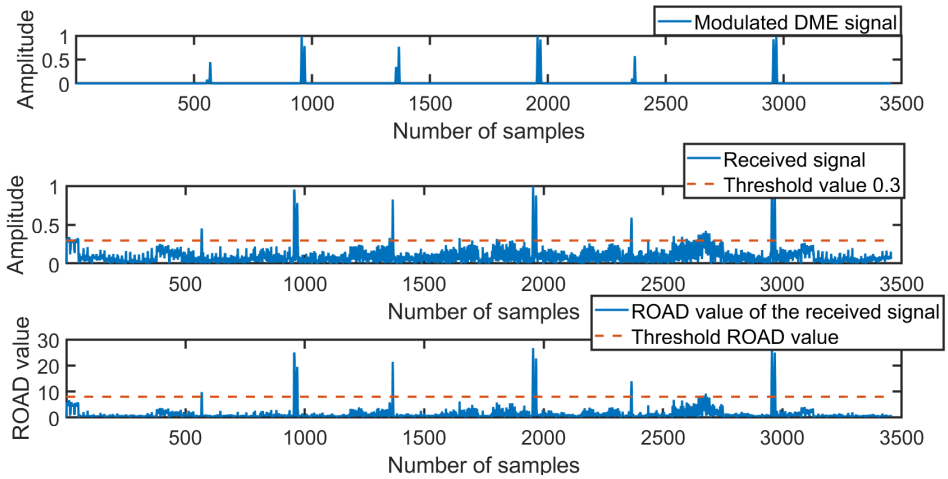

Figure 9. DME interference (**Top**), amplitude of the received signal without interference mitigation (**Middle**) and ROAD value of the received signal (**Bottom**) for an SNR of 15 dB.

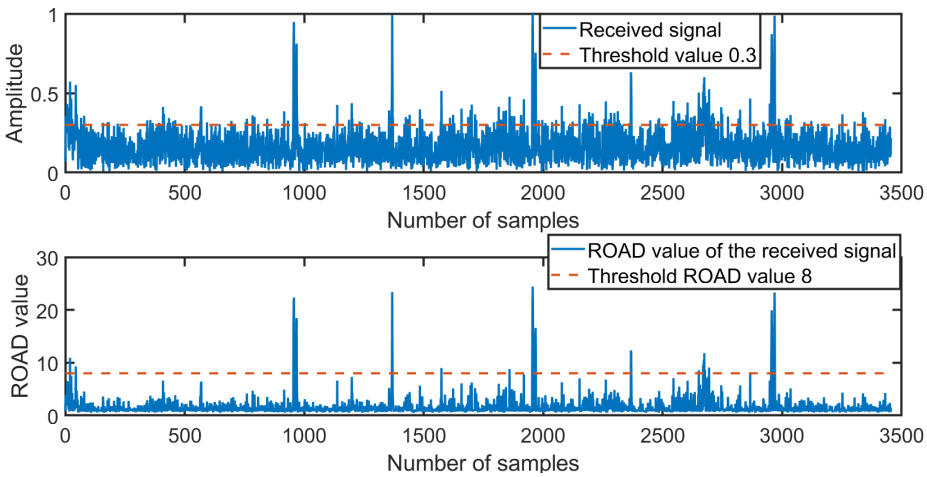

Figure 10. Amplitude of the received signal without interference mitigation and ROAD value of the received signal for an SNR of 0 dB.

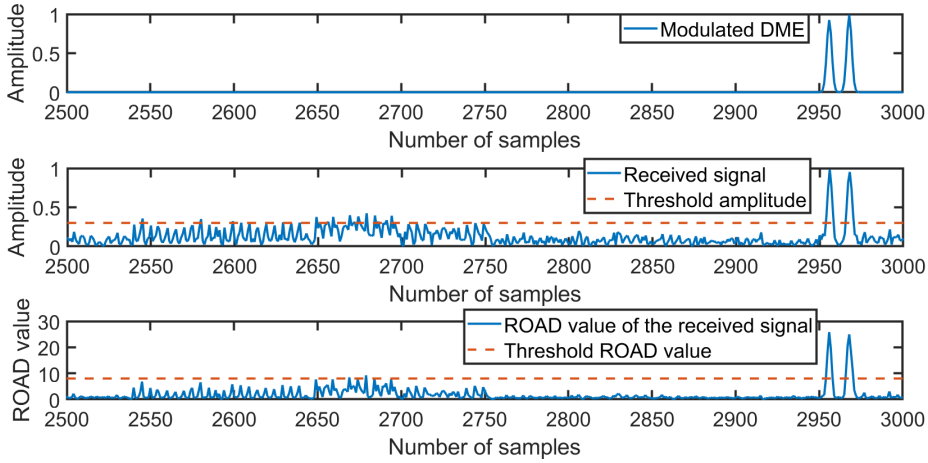

Figure 11. DME interference (**Top**), amplitude of the received signal without interference mitigation (**Middle**) and ROAD value of the received signal (**Bottom**) for an SNR of 15 dB.

An inclusive analysis of amplitude-based sensing and ROAD value-based sensing at low and high SNR levels has been portrayed in Figures 12 and 13, respectively. The characterization of different probability measures (accuracy, false detection and missed detection) are also analyzed in Figures 14–16. The findings from the comparative study of amplitude-based sensing and ROAD value-based sensing are as follows:

1. The number of false detections in amplitude-based sensing is more at a low SNR level of operation than high SNR values.
2. The number of false detections due to ROAD value-based sensing is always less (whether in high SNR level or in low SNR level) than amplitude-based sensing.
3. The performance of ROAD value-based sensing is almost the same in both low and high SNR levels.
4. ROAD value-based sensing shows some amount of missed detection as in between the samples 1000 and 1500 (Figure 13). The same sample is not lost in amplitude-based detection as it crosses the threshold value.
5. The probability of false detection that occurs in ROAD value-based sensing is observed to be always less than from amplitude-based sensing for all the SNR values under consideration. The probability of false detection is found to be decreased with an increase in SNR values due to the reduction in noise level (Figure 15).
6. The probability of missed detection is observed to increase with an increase in SNR levels in the case of amplitude-based sensing (Figure 16).
7. The probability of missed detection is found to be slightly decreasing with an increase in SNR values for ROAD value-based detection (Figure 16).
8. The probability of missed detection is found to be more for ROAD value-based detection than amplitude-based sensing.
9. Regardless of the elevated number of missed detections that occurred in ROAD value-based sensing, the method showed high accuracy in detection compared to conventional amplitude-based sensing (Figure 14).

The above mentioned (2, 3, 5 and 9) statements, which are realized from the obtained results, affirm that ROAD value-based sensing is admirable in comparison to amplitude value-based sensing in detecting DME interference.

Furthermore, the characterization of the ROAD statistic-based detection for different threshold ROAD values and SNRs has been performed. The results are as displayed in Figures 17–19. It has been observed that the probability of false detection decreases with an increase in threshold values (Figure 17) and the probability of missed detection increases with an increase in threshold value, Figure 18. Hence, there is a trade-off between false detection and missed detection for different values of threshold. Hence, to identify the optimum threshold, we have analyzed the variation in probability of correct detection

(accuracy) for different threshold values. From Figure 19, it is noted that the accuracy in ROAD value-based sensing increases from threshold ROAD value 5 to 8. The reason for this nature is the considerable reduction in false detection occurring in ROAD value-based sensing. Further, the performance starts diminishing from 8 to 12. This can be due to the increase in missed detection that occurs for high threshold value.

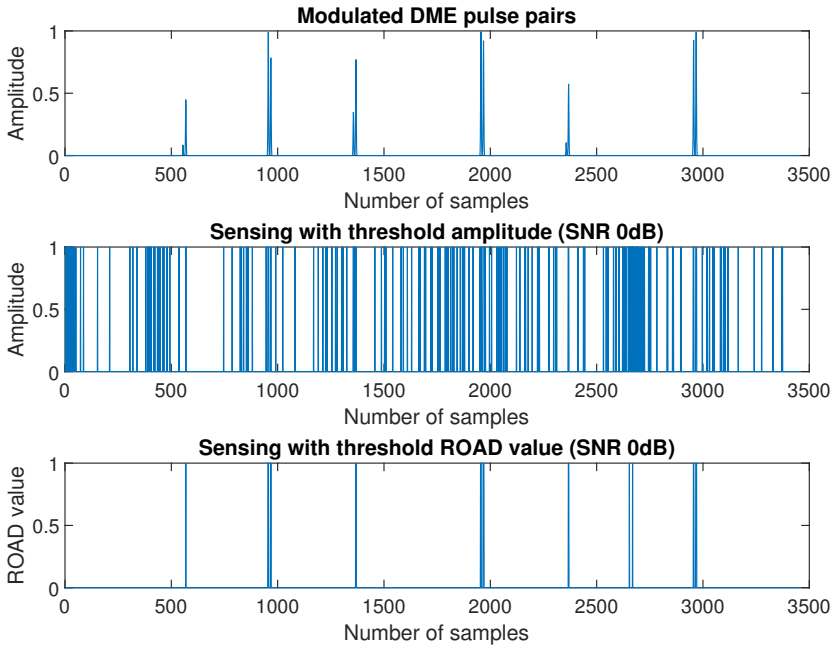

Figure 12. DME interference (**Top**), threshold amplitude-based sensing (**Middle**) and threshold ROAD value-based sensing (**Bottom**) for an SNR of 0 dB.

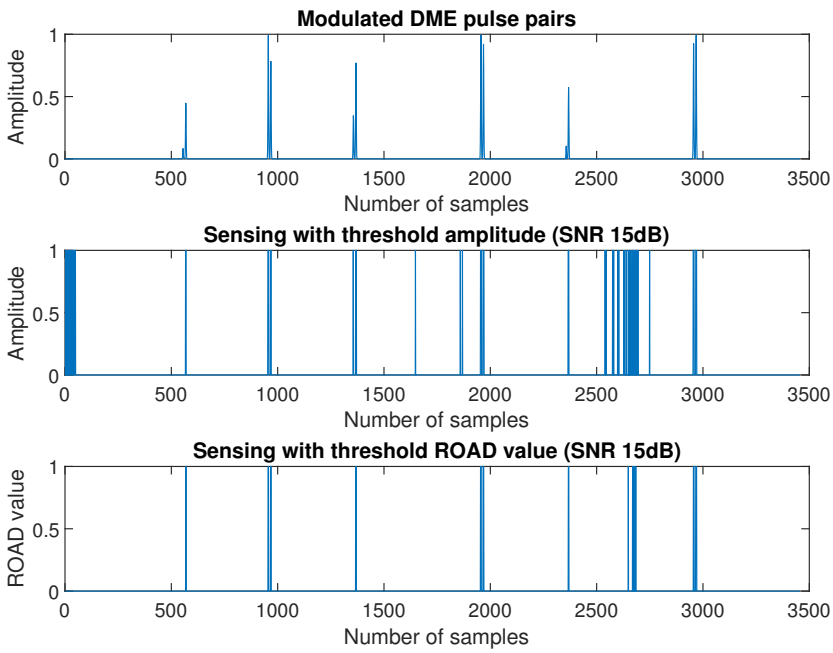

Figure 13. DME interference (**Top**), threshold amplitude-based sensing (**Middle**) and threshold ROAD value-based sensing (**Bottom**) for an SNR of 15 dB.

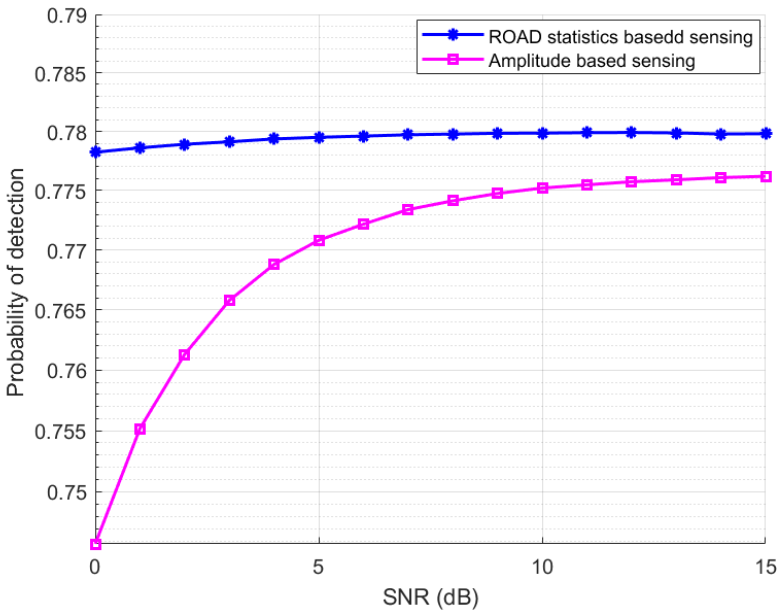

Figure 14. Probability of detection vs. SNR.

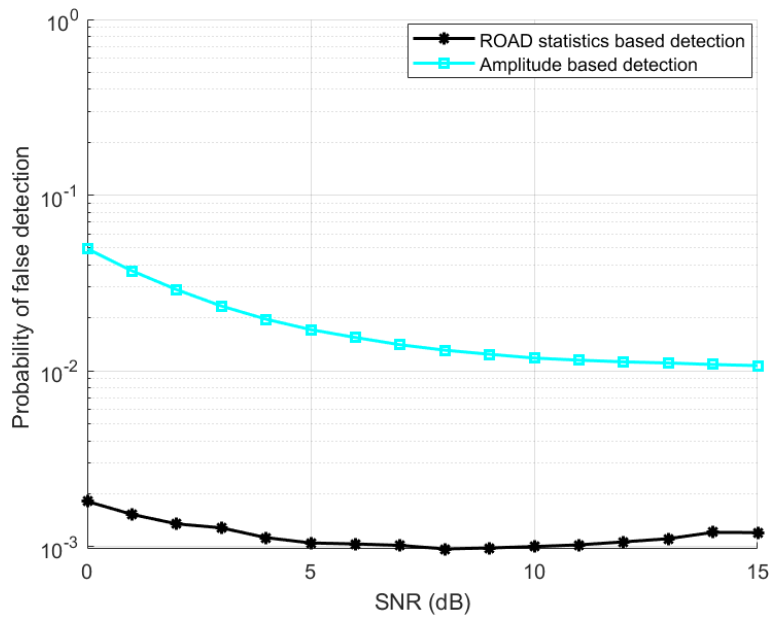

Figure 15. Probability of false detection vs. SNR.

For better clarity of the results, the variation in probability of false detection and missed detection has been plotted for a constant SNR value. The rate of decrease in false detection with the increase in threshold value is clearly visible in Figure 20. The variation in accuracy and missed detection are separately plotted to verify the optimum threshold value of detection and the reason behind it. From Figure 21, it is evident that optimum threshold value of detection is occurring for a value of 8. The reduction in detection after threshold value 8 is due to the increase in missed detection as in Figure 22.

Once the significance of ROAD value-based sensing and its optimum threshold ROAD value are identified (based on experimental results), the method is incorporated with an existing pulse blanking method to propose a new DME mitigation scheme.

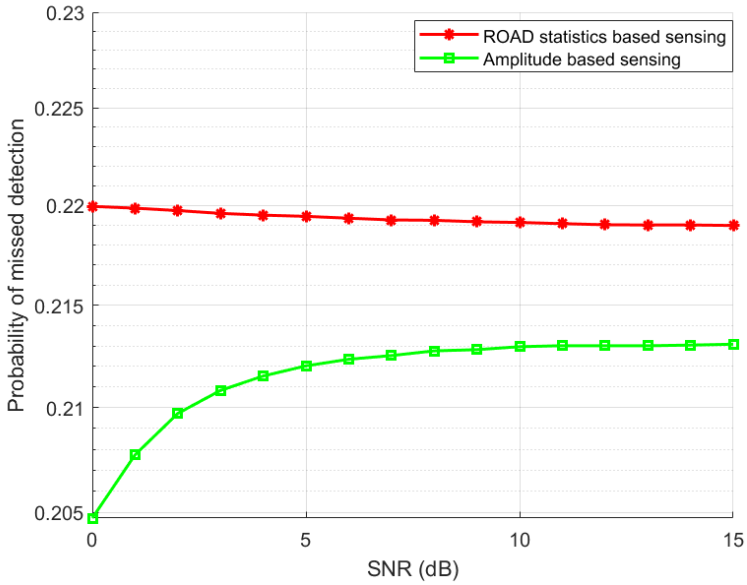

Figure 16. Probability of missed detection vs. SNR.

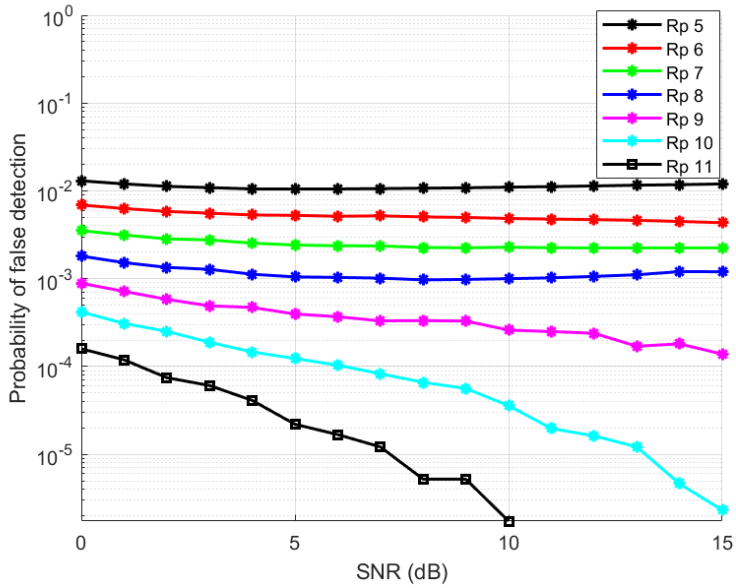

Figure 17. Probability of false detection in ROAD statistics-based detection for different threshold value vs. SNR.

The block diagram of the proposed LDACS receiver is shown in Figure 4. Initially, the cyclic prefix bits are removed from the received data. The resulting data are then converted into frequency domain using fast Fourier transform. Further, the frame decomposer separates the pilot symbols and complex data from the corresponding subcarriers. The segregated complex data values further undergo QPSK demodulation and symbol de-mapping to obtain the bitstreams. The bitstreams are de-interleaved and decoded using de-interleaver and vitterbi decoder, respectively. From the output of the vitterbi decoder, redundant bits are removed and decoded using the RS decoder to obtain the original data.

Figure 23 shows the variation in BER with different transmit SNR values. It has been observed that the proposed ROAD PB exhibits a much improved performance for a threshold value of 8. Figure 24 shows the variation in performance of ROAD PB for different threshold values ranging from 7 to 11. The performance of ROAD PB initially improved with a rise in threshold values and then started diminishing. The reason for this nature

is very obvious; ROAD detectors with low threshold values perceive the small variations from the neighboring carrier as DME interference. The actual data can cause a variation in ROAD values which can lead to false detection of DME interference. Moreover, once DME interference is detected in a subcarrier with a low threshold value, blanking the subcarrier causes the loss of more data. As OFDM systems have a self-removal noise mechanism due to the principle of orthogonality, the focus of detection is for large variation. Hence, there is an optimum high threshold value for which leaving the data is better than maintaining or estimating. From the results shown in Figure 24, the optimum threshold value is noted as 8. The accuracy of interference detection starts diminishing for a threshold value greater than an optimum threshold value. In this situation, the ROAD interference detector will only sense a very large variation from the neighboring carrier as DME interference leading to missed detection.

With the introduction of pulse blanking, a possibility of change in optimum threshold exists, if one considers the trade-off between interference power and signal distortion. Excess interference power may exist in mitigated data if the threshold value is high. On the other hand, reducing the threshold value can cause more distortion and loss of data due to blanking. In our work, the optimum threshold value of ROAD value-based sensing is recognized as the optimum value of operation to obtain data with minimum BER (Figures 21 and 24). As ROAD value-based noise detection is more accurate than the conventional amplitude-based method, it introduces less distortion in the mitigated data and prevents the extra loss of falsely detected data.

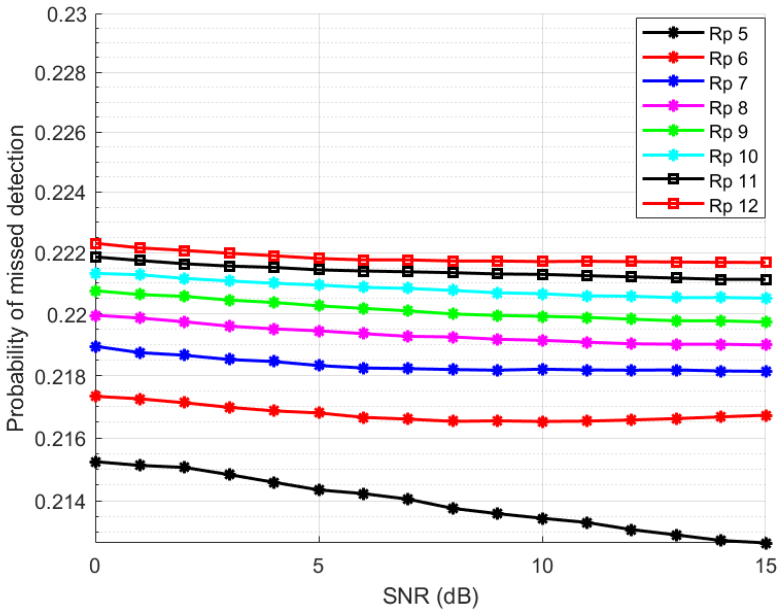

Figure 18. Probability of missed detection in ROAD statistics-based detection for different threshold value vs. SNR.

The performance of the proposed ROAD PB is further compared with GAE enhanced pulse peak processors and the results are as shown in Figure 25. The proposed ROAD PB outperformed the GAE enhanced pulse peak attenuators and limiters (Type I and II). Similarly, Figure 26 depicts the performance comparison of the proposed ROAD PB with OBE enhanced pulse peak processors. It has been observed that ROAD PB could outperform OBE PPA. Moreover, ROAD PB has similar or slightly better performance than OBE PPLs for low SNR values. For SNR values 8 dB and above, OBE enhanced pulse peak limiters performed better than ROAD PB. Figure 27 compares the performance of ROAD PB with pulse blanking, GAE PPL (Type 2) and OBE PPL (Type 2). It has been observed that GAE PPL and OBE PPL have an improved performance compared to pulse blanking as data estimation has been performed instead of blanking the noise affected

signal. The threshold value used for all types of pulse peak processors is 0.3 [30]. When ROAD statistics is incorporated with pulse blanking, the performance could be improved better than GAE PPL and comparable performance with OBE PPL.

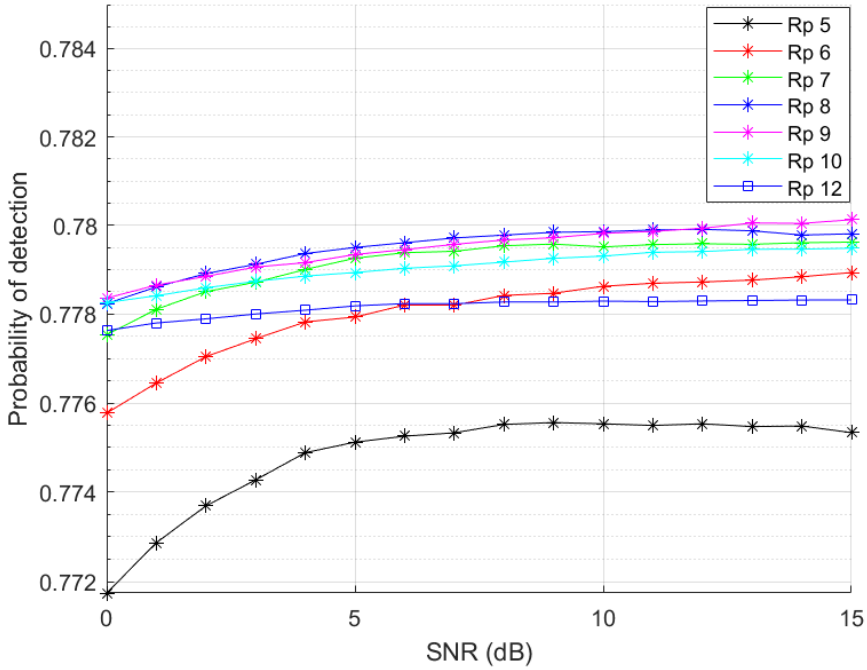

Figure 19. Accuracy in ROAD statistics-based detection vs. SNR.

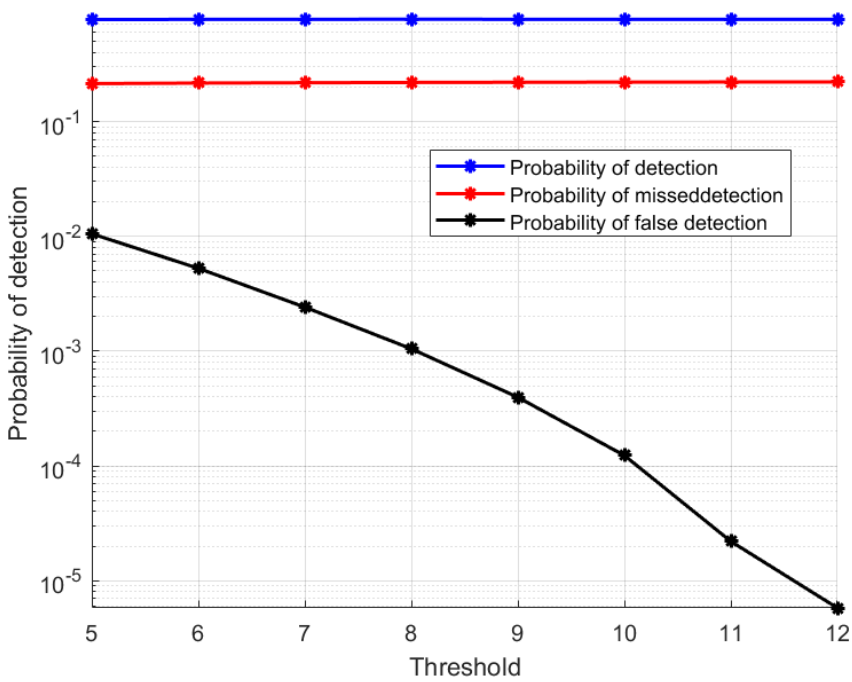

Figure 20. Probability of detection vs. threshold for SNR = 5 dB.

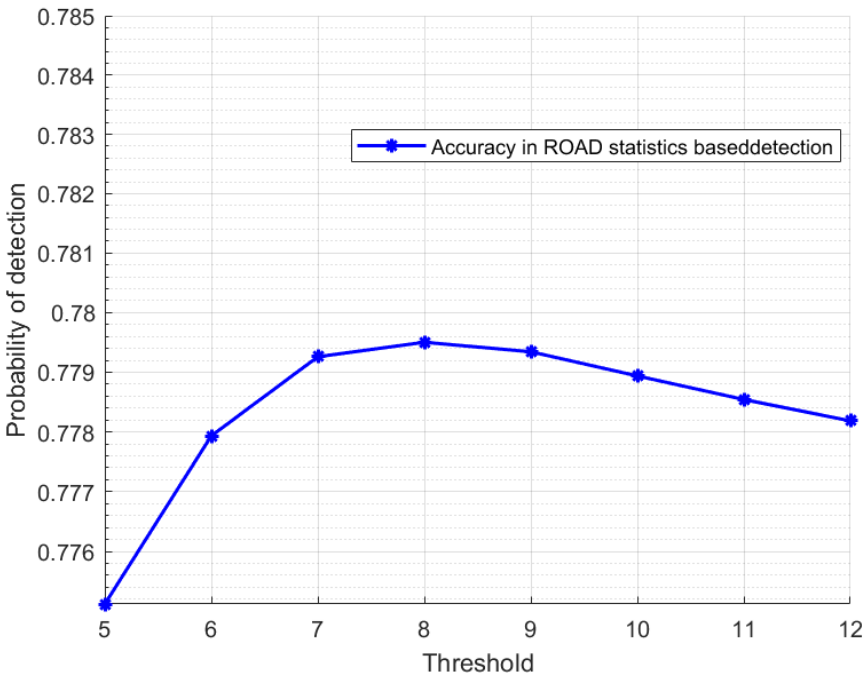

Figure 21. Accuracy in ROAD statistics-based detection (SNR = 5 dB) vs. threshold.

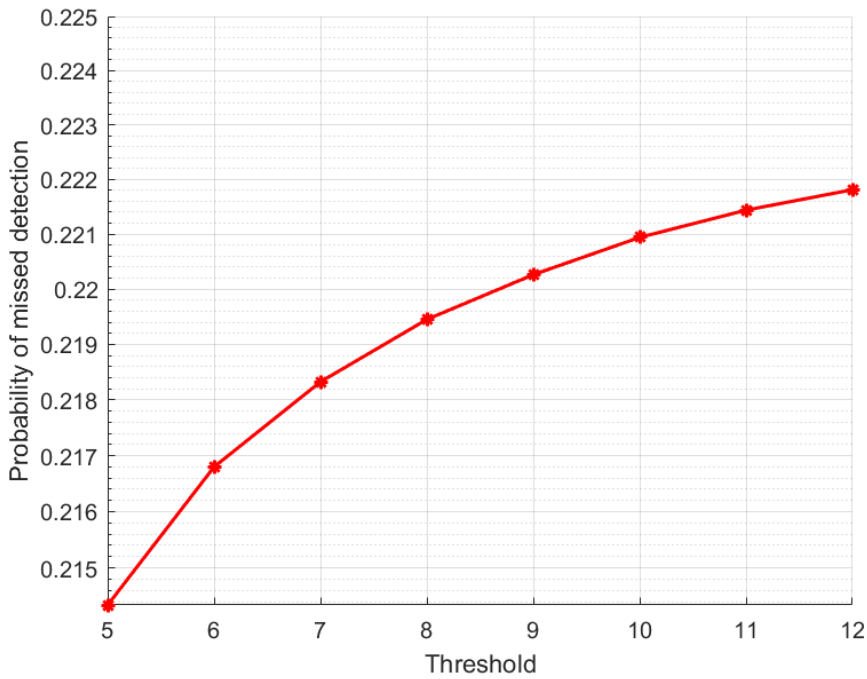

Figure 22. Probability of missed detection in ROAD statistics-based sensing (SNR = 5 dB) vs. threshold.

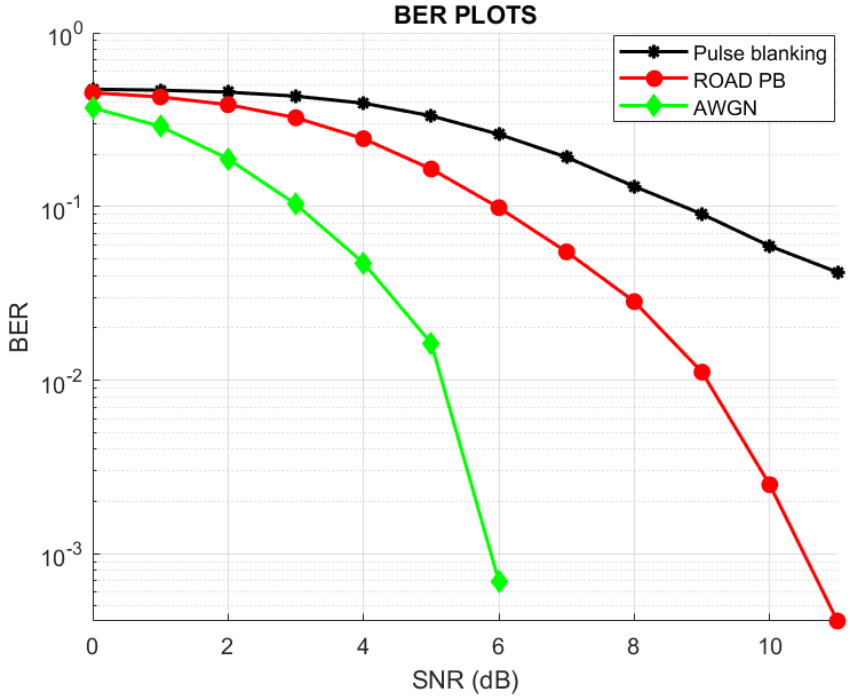

Figure 23. Performance of ROAD PB vs. pulse blanking.

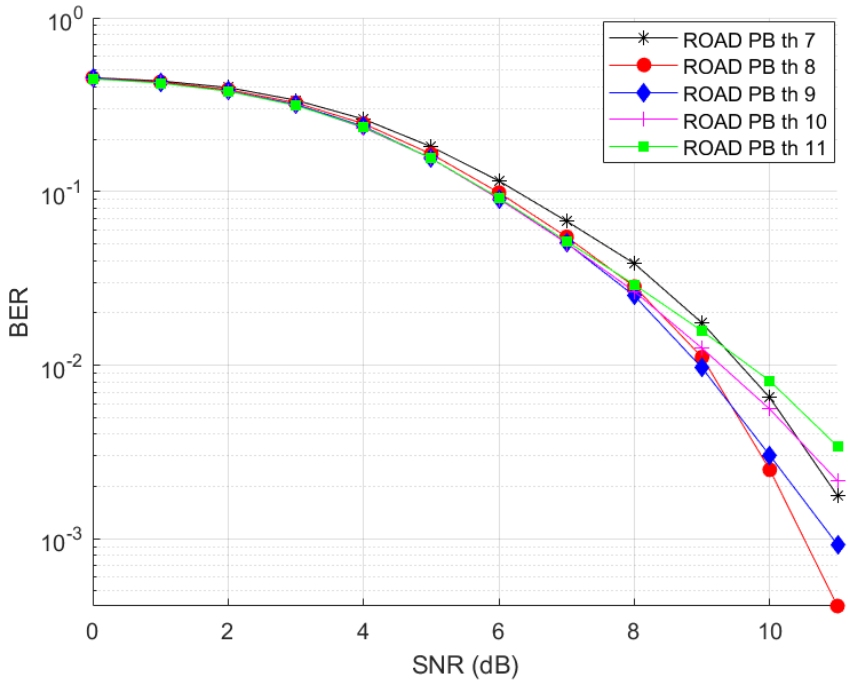

Figure 24. Variation of ROAD PB with different threshold value.

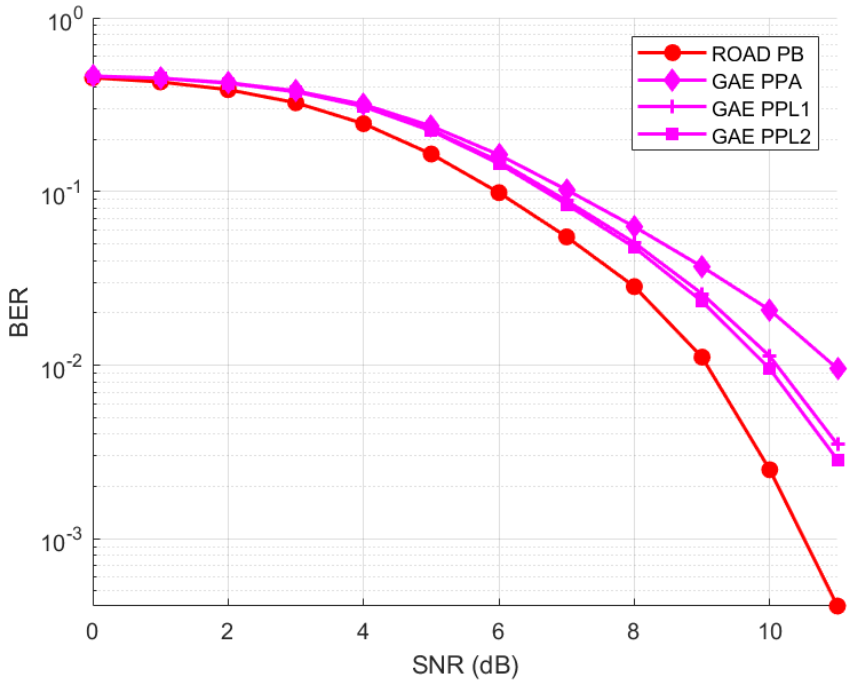

Figure 25. Performance of ROADPB vs. GAE enhanced pulse peak processors.

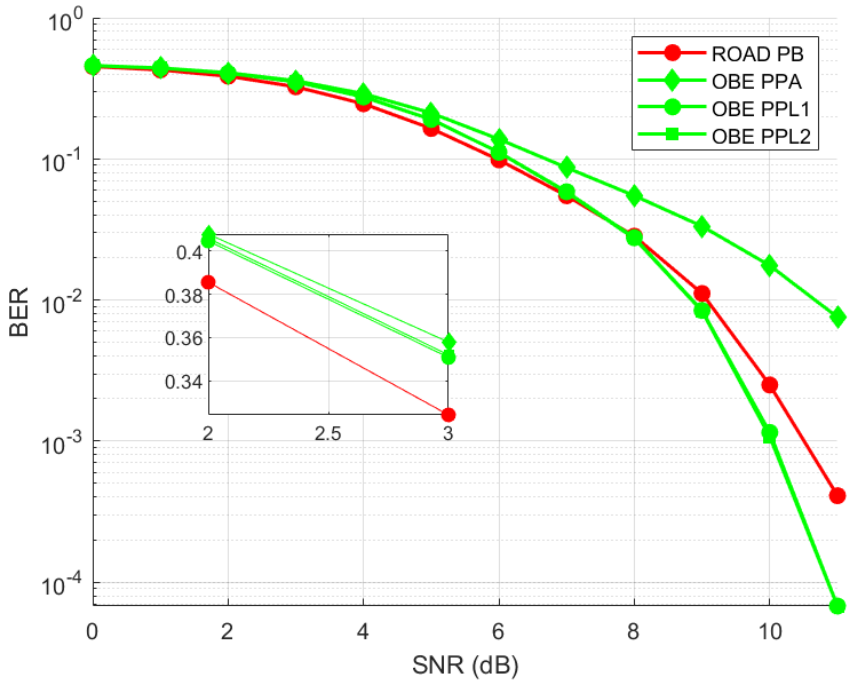

Figure 26. Performance of ROADPB vs. OBE enhanced pulse peak processors.

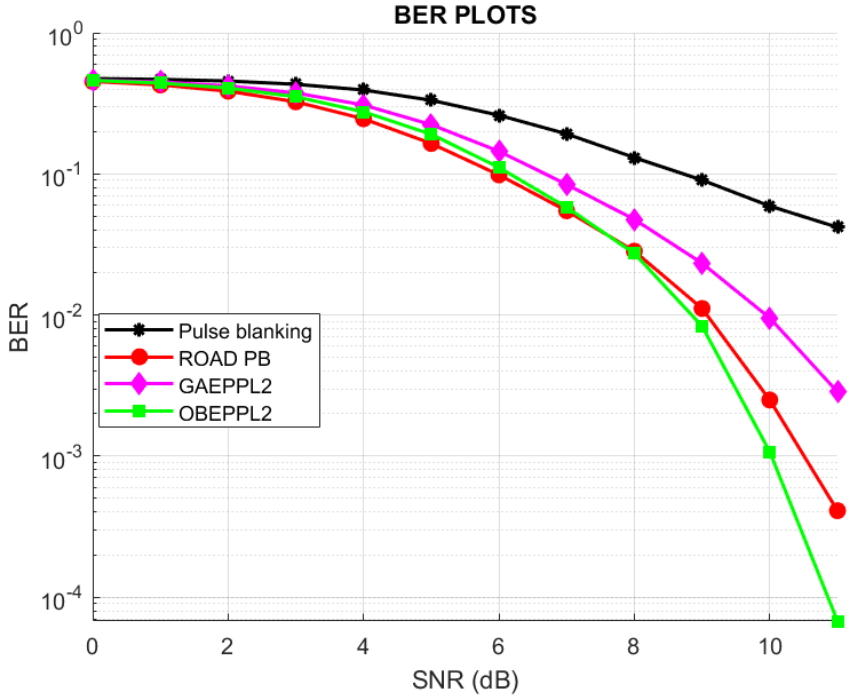

Figure 27. Performance of ROADPB vs. pulse blanking, GAE and OBE enhanced pulse processors.

Table 1. OFDM Parameters for LDACS1 [9].

OFDM Parameters	Values
Effective RF BW (FL or RL)	498.05 KHz
FFT size N_{FFT}	64
Sampling time T_{sa}	1.6 µs
Subcarrier spacing f	9.765625 KHz
Used subcarriers N_u	50
Useful symbol time N_u	102.4 µs
Cyclic prefix time T_{cp}	17.6 µs
Total OFDM symbol time T_s	120 µs
Guard time T_g	4.8 µs
Windowing time T_w	12.2 µs
Number of lower frequency guard subcarriers $N_{g,left}$	7
Number of higher frequency guard subcarriers	
Lower frequency guard subcarriers $N_{g,right}$	6
Total FFT BW B_g	625 KHz

6. Conclusions

In this paper, a new DME mitigation scheme named ROAD PB is proposed to mitigate the DME interference using pulse blanking. The ROAD PB detects DME interference with a method named ROAD statistics-based detection. The method detects the interference from the ROAD values of the received signal. The performance of the new detection method is compared with the conventional amplitude-based sensing method. The results guided to the following conclusions:

1. ROAD statistics detection method outperformed conventional amplitude-based sensing in identifying the location of the DME interference (Figure 11).
2. The probability of detection of ROAD value-based sensing remains the same for both low and high SNR values, whereas the same found be varying for amplitude-based sensing. The accuracy of detection of the proposed method always excelled over conventional amplitude-based sensing (Figure 14).

3. Though ROAD value-based sensing showed an increase in missed detection in comparison to amplitude-based sensing, the method could always achieve enlarged accuracy due to the substantial decrease in false detection. For an SNR value of 0 dB, regardless of the 2% increase in probability of missed detection compared to amplitude-based sensing, the proposed method achieved a 3% increase in probability of detection (accuracy) with the help of a 4% reduction in the probability of false detection (Figures 14–16).
4. The ROAD statistic-based interference sensing always shows a considerable reduction in false detection of the DME signal.
5. The optimum threshold value of detection is observed to be 8. The reduction in performance for a threshold value lower than 8 is due to the presence of more numbers of false detection than threshold 8. The reduction in performance for a threshold value higher than 8 is due to the increase in missed detection at higher threshold values.

From the results obtained with the comparative study of the proposed method (ROADPB) with amplitude-based detection methods such as pulse blanking and pulse peak processors, we observed the following:

1. ROAD PB exhibited improved performance than the pulse blanking method which uses the amplitude of the received signal for the detection of DME interference.
2. ROAD PB always outperformed the three types of GAE enhanced pulse peak processors in its optimum threshold value of operation.
3. ROAD PB showed better performance than OBE enhanced pulse peak attenuator and comparable performance with OBE enhanced pulse peak limiters.

In comparison to pulse blanking, ROAD PB could achieve the SNR saving of 2.7 dB at a BER of 10^{-1} by introducing some amount of complexity in the receiver. Moreover, at a BER of 10^{-1}, ROAD PB could accomplish SNR savings of 2.7, 1.1, 0.7, 0.25 and 0.2 dBs compared to GAEPPA, GAEPPL, OBEPPA and OBEPPL, respectively. The proposed ROAD PB is significant due to its improved performance at low SNR regions in comparison to pulse blanking. Moreover, ROAD value-based detection can be used to sense impulse noise in any type of OFDM-based communication systems where threshold-based detection can be used. In the future, ROAD value-based detection can be incorporated with any other threshold-based DME mitigation scheme such as GAE enhanced methods. ROAD PB-based LDACS receiver can be extended for the en-route channel. The performance of this method in LDACS RL can also be analyzed. Though this method is investigated on the LDACS background, the method is compatible in cutting down impulse noise in any OFDM-based communication systems.

Author Contributions: Conceptualization, M.K. and R.M.; methodology, M.K. and R.M.; software, M.K.; validation, A.R.and R.M.; formal analysis, M.K.; writing—original draft preparation, writing—review and editing, M.K.; supervision, R.M. and A.R. All authors have read and agreed to the published version of the manuscript.

Funding: This research received no external funding.

Institutional Review Board Statement: Not applicable.

Informed Consent Statement: Not applicable.

Data Availability Statement: Exclude this statement.

Conflicts of Interest: The authors declare no conflict of interest.

Nomenclature

GAE	Genie-aided estimator
OBE	Optimal Bayesian estimator
LDACS	L-band Digital Aeronautic Communication Systems
DME	Distance measuring equipment

PPA	Pulse peak attenuator
PPL	Pulse peak limiter
GAEPPA	Genie-aided estimator enhanced pulse peak attenuator
GAEPPL	Genie-aided estimator enhanced pulse peak limiter
OBEPPA	Optimal Bayesian estimator enhanced pulse peak attenuator
OBEPPL	Optimal Bayesian estimator enhanced pulse peak limiter
WAIC	Wireless avionic intra communication
UAV	Unmanned aerial vehicle
A/G	Air–ground communications
DSB-AM	Double sideband amplitude modulation
ATM	Air traffic management
TBO	Trajectory-based operations
ICAO	International civil aviation organization
GSM	Global system for mobile communication
TACAN	Tactical air navigation
JTIDS	Joint tactical information distribution system
UAT	Universal access transceiver
SSR	secondary surveillance radar
ACAS	airborne collision avoidance system
FL	Forward link
GS	Ground station
RL	Reverse link
AS	Air station
FDD	Frequency division duplexing
CCK	Complementary code keying
DWT	Discrete wavelet transform
PLC	Power-line communication
ADSL	Asymmetric digital subscriber lines
DVBT	Digital video broadcasting—terrestrial
QPSK	Quadrature Phase Shift Keying
AWGN	Additive white Gaussian noise
K-GMM	K-component Gaussian mixture mode
F	LDACS forward link frame
F_t	tth symbol of LDACS forward link frame (F)
σ_F^2	variance of F_t
N	Number of orthogonal subcarriers
S_t	The OFDM symbol
N_{CP}	number of cyclic prefix bits
X'_t	Transmitted vector
X'	Transmitted signal
r'	Received signal
i_t	Noise
A_t	AWGN noise
p_t	Impulse noise
r'_t	Received signal at an instant 't'
r_t	Received signal after CP removal 't'
$P_d(t)$	A pair of DME pulses
$I_{pd}(f)$	Modulated DME spectrum
$I_{pd}(t)$	DME interfering signal to LDACS system
t	Output signal at each time epoch
$\hat{x}_t$	Estimated output signal at each time epoch
$\sigma^2 X$	Signal power of transmitted signal X'
$\sigma^2 i$	Noise power added to transmitted signal
$\sigma^2 X_t$	Transmitted signal power at an instant
$\sigma^2 i_t$	Noise power at an instant
P_k	Probability of occurrence of each Gaussian component k
Γ	The ratio of thermal noise to impulse noise
pI	Probability of impulse noise

$\sigma^2 I$	Impulse noise power
$\sigma^2 0$	Thermal noise power
$\hat{x}_{\|kPA\|}(y)$	Output of GAEPPA
$\hat{x}_{\|kPL\|}(y)$	Output of GAEPPL Type 1
$\hat{x}_{\|kPLs\|}(y))$	Output of GAEPPL Type 2
ρ_k	Attenuation factor for GAEPPA
ρ_{mod}	Attenuation factor for GAEPPL Type 1
$\hat{x}_{\|kOPA\|}(y)$	Output of OBEPPA
$\hat{x}_{\|kOPL\|}(y)$	Output of OBEPPL (Types 1 and 2)
$\beta_o(y)$	Attenuation factor for OBEPPA and JOBEPPA
$\beta_{mod}(y)$	Attenuation factor for OBEEPPL
μ	General scaling factor

Appendix A

Following, we provide the derivation of extra computational complexity introduced by ROAD PB, Section 4.1.

Appendix A.1

The extra computational complexity put forward by ROAD PB compared to conventional pulse blanking is the sum of the computational complexity put forward by the steps to calculate ROAD value. The following steps are used to calculate ROAD value of a center sample in one OFDM symbol:

1. The received OFDM symbol for each time epoch is considered as a one-dimensional vector. For a one-dimensional vector of size (1 × N), the absolute difference between a center sample and a receiving sample for each time epoch $f_d(k)$ are calculated as in (A1)

$$f_d(k) = |r_k - [r_{k-fracN-1/2}, ..., r_{k+frac(N-1)/2}]| \tag{A1}$$

   No complex multiplications are introduced in this step.
   Here, the number of complex additions put forward is $N-1$ for center sample or for one subcarrier. It is the same as that of $(2 \cdot N - 1)$ real multiplications.
   Thus, for N number of subcarriers, the number of complex additions involved in the calculation of absolute difference from a center sample C_a^d is as follows,

$$C_a^d = N \cdot (N-1). \tag{A2}$$

   It is the same as $2N \cdot (2 \cdot N - 1)$ real additions and can be expressed as in (A3)

$$R_a^d = 2N \cdot (2N-1). \tag{A3}$$

2. The difference vector $(f_d(k))$ is sorted in increasing order.

$$Q(k) = sort(f_d(k)). \tag{A4}$$

   No complex multiplications or additions are introduced in this step.
   For a one-dimensional vector of size N, the number of real-time additions put forward by sorting depends on the type of sorting that is used. For instance, if selective sorting is used, it introduces $\frac{N \cdot (N-1)}{2}$ number of real-time additions for a single center sample. Thus, for N number of samples, the number of real-time additions involved in selective sorting is as in (A5)

$$R_a^s = \frac{N^2 \cdot (N-1)}{2}. \tag{A5}$$

3. The ROAD value is calculated as the sum of first $(N-1)/2$ values of $Q(k)$

$$ROAD = \Sigma_{k=1}^{(N-1)/2} Q(k). \tag{A6}$$

No complex multiplications or additions are introduced in this step.
Finally, the number of real-time additions put forward by adding the first half values of the sorted output is $\frac{(N-1)}{2}$.
For N number of samples, the number of real-time additions involved is as in (A7)

$$R_a^a = \frac{N \cdot (N-1)}{2}. \tag{A7}$$

References

1. EUROCONTROL. EUROCONTROL's Challenges of Growth 2018 Study Report. Available online: https://www.eurocontrol.int/sites/default/files/2019-07/challenges-of-growth-2018-annex1-0.pdf (accessed on 29 September 2019).
2. Available online: https://www.ldacs.com/wp-content/uploads/2013/12/ACP-DCIWG-IP01-LDACS-White-Paper.pdf (accessed on 11 November 2021).
3. L-DACS1 System Defenition Proposal: Deliverable D2. 2009. Available online: Https://www.ldacs.com/wp-content/uploads/2014/02/LDACS1-Specification-Proposal-D2-Deliverable.pdf (accessed on 11 November 2021).
4. L-DACS2 System Defenition Proposal: Delivrable D2, (EUROCONTROL, Brussels, Belgium, 2009) Tech. Rep. 1.0, Version 1. Available online: https://www.eurocontrol.int/sites/default/files/2019-05/11052009-ldcas2-d2-deliverable-v1.0.pdf (accessed on 11 November 2021).
5. Epple, U.; Schnell, M. Mitigation of impulsive interference for LDACS1—Potentials of blanking nonlinearity. In Proceedings of the 2015 Integrated Communication, Navigation and Surveillance Conference (ICNS), Herdon, VA, USA, 21–23 April 2015; pp. 1–16.
6. Mostafa, M.; Schnell, M. DME-compliant LDACS1 cell planning: Initial steps. In Proceedings of the 2015 Integrated Communication, Navigation and Surveillance Conference (ICNS), Herdon, VA, USA, 21–23 April 2015; pp. 1–42.
7. Schnell, M.; Epple, U.; Shutin, D.; Schneckenburger, N.T. LDACS: Future aeronautical communications for air-traffic management. *IEEE Commun. Mag.* **2014**, *52*, 104–110. [CrossRef]
8. Thiasiriphet, T.; Schneckenburger, N.; Schnell, M. Impact of the DME interference on the LDACS1 ranging performance. In Proceedings of the 28th International Technical Meeting of the Satellite Division of The Institute of Navigation (ION GNSS+ 2015), Tampa, FL, USA, 18 September 2015; pp. 1446–1467.
9. Muthalagu, R.T. Mitigation of DME interference in LDACS1-based future air-to-ground (A/G) communications. *Cogent Eng.* **2018**, *5*, 1472199. [CrossRef]
10. Agrawal, N.; Darak, S.J. Performance analysis of reconfigurable filtered OFDM for LDACS. In Proceedings of the 2019 11th International Conference on Communication Systems & Networks (COMSNETS), Bengaluru, India, 7 January 2019; pp. 500–503.
11. Agrawal, N.; Darak, S.J.; Bader, F. Spectral Coexistence of LDACS and DME: Analysis via Hardware software co-design in presence of real channels and RF impairments. *IEEE Trans. Veh. Technol.* **2020**, *69*, 9837–9848. [CrossRef]
12. Agrawal, N.; Darak, S.J.; Bader, F. New Spectrum Efficient Reconfigurable Filtered-OFDM Based L-Band Digital Aeronautical Communication System. *IEEE Trans. Aerosp. Electron. Syst.* **2019**, *55*, 1108–1122. [CrossRef]
13. Mathew, L.K.; Vinod, A.P. An energy-difference detection based spectrum sensing technique for improving the spectral efficiency of LDACS1 in aeronautical communications. In Proceedings of the 2016 IEEE/AIAA 35th Digital Avionics Systems Conference (DASC), Sacramento, CA, USA, 25–29 September 2016; pp. 1–5.
14. Mathew, L.K.; Vinod, A.P.; Madhukumar, A.S. A cyclic prefix assisted spectrum sensing method for aeronautical communication systems. In Proceedings of the 2019 IEEE International Symposium on Circuits and Systems (ISCAS), Sapporo, Japan, 26–29 May 2019; pp. 1–5.
15. Raja, M. Application of cognitive radio and interference cancellation in the L-Band based on future air-to-ground communication systems. *Digit. Commun. Netw.* **2019**, *5*, 111–120. [CrossRef]
16. Epple, U.; Schnell, M. Overview of interference situation and mitigation techniques for LDACS1. In Proceedings of the 2011 IEEE/AIAA 30th Digital Avionics Systems Conference, Seattle, WA, USA, 16–20 October 2011; p. 4C5-1.
17. Wang, H.; Liu, R. DME/TACAN interference mitigated by mixed blanking in B2 band. In Proceedings of the 2011 IEEE 13th International Conference on Communication Technology, Jinan, China, 25–28 September 2011; pp. 897–900.
18. Bai, Y.; Zhang, X.; Zhao, L. Co-channel CCK transmission overlapped with DME in aeronautical communication. In Proceedings of the 2014 IEEE China Summit & International Conference on Signal and Information Processing (ChinaSIP), Xi'an, China, 9–13 July 2014; pp. 403–406.
19. Li, Q.; Zhang, J.; Xie, J.; Mostafa, M.; Schnell, M. Iterative interference mitigation and channel estimation for LDACS1. In Proceedings of the 2014 IEEE/AIAA 33rd Digital Avionics Systems Conference (DASC), Colorado Springs, CO, USA, 5–9 October 2014; p. 3B2-1.

20. Hirschbeck, M.; Huber, J.B. Block based frequency selective mitigation of pulsed interference in the L-band. In Proceedings of the 10th International ITG Conference on Systems, Communications and Coding, Hamburg, Germany, 2–5 February 2015; pp. 1–6.
21. Li, D.; Wu, Z.T. DME Interference mitigation for L-DACS1 based on system identification and sparse representation. *Chin. J. Aeronaut.* **2016**, *6*, 1762–1773. [CrossRef]
22. Saaifan, K.A.; Henkel, W. Lattice signal sets to combat pulsed interference from aeronautical signals. In Proceedings of the 2011 IEEE International Conference on Communications (ICC), Kyoto, Japan, 5–9 June 2011; pp. 1–5.
23. Abd-Elaty, E.; El-Agooz, S.; Zekry, A.E. Compact Spread Spectrum LDACS Wavelet Based for DME Interference Mitigation. In Proceedings of the 2019 36th National Radio Science Conference (NRSC), Port Said, Egypt, 16–18 April 2019; pp. 259–265.
24. Abd-Elaty, E.; Zekry, A.; El-Agooz, S.; Helaly, A.M. Nested code division multiple access for distance measuring equipment interference mitigation in L-band digital aeronautical communication system. *Int. J. Commun. Syst.* **2021**, *34*, e4804. [CrossRef]
25. Muthalagu, M.K.R.; Mathew, L.K.; Rajak, A. Deep Clipping Based Interference Mitigation Technique for LDACS. In Proceedings of the 2021 IEEE/AIAA 40th Digital Avionics Systems Conference (DASC), San Antonio, TX, USA, 3–7 October 2021; pp. 1–6. [CrossRef]
26. Eriksson, H.B.; Ödling, P.; Koski, T.; Börjesson, P.O. A genie-aided detector with a probabilistic description of the side information. In Proceedings of the 1995 IEEE International Symposium on Information Theory, Whistler, BC, Canada, 17–22 September 1995; p. 332.
27. Rožić, N.; Banelli, P.; Begušić, D.; Radić, J.T. Multiple-Threshold Estimators for Impulsive Noise Suppression in Multicarrier Communications. *IEEE Trans. Signal Process.* **2018**, *10*, 1619–1633. [CrossRef]
28. Banelli, P. Bayesian estimation of a Gaussian source in Middleton's class—A impulsive noise. *IEEE Signal Process. Lett.* **2013**, *20*, 956–959. [CrossRef]
29. Banelli, P.; Rugini, L. Impulsive noise mitigation for wireless OFDM. In Proceedings of the 2015 IEEE 16th International Workshop on Signal Processing Advances in Wireless Communications (SPAWC), Stockholm, Sweden, 28 June–1 July 2015; pp. 346–350.
30. Keshkar, M.; Muthalagu, R.; Rajak, A.; Mathew, L.K. GAE and OBE Enhanced Interference Mitigation Techniques in LDACS. *Aerospace* **2022**, *9*, 45. [CrossRef]
31. Garnett, R.; Huegerich, T.; Chui, C.; He, W. A universal noise removal algorithm with an impulse detector. *IEEE Trans. Image Process.* **2005**, *14*, 1747–1754. [CrossRef] [PubMed]
32. Barazideh, R.; Niknam, S.; Natarajan, B. Impulsive Noise Detection in OFDM-based Systems: A Deep Learning Perspective. In Proceedings of the 2019 IEEE 9th Annual Computing and Communication Workshop and Conference (CCWC), Las Vegas, NV, USA, 7–9 January 2019; pp. 0937–0942. [CrossRef]
33. Gao, G.X. DME/TACAN Interference and its Mitigation in L5/E5 Bands. In Proceedings of the 20th International Technical Meeting of the Satellite Division of the Institute of Navigation (ION GNSS 2007), Fort Worth, TX, USA, 28 September 2007; pp. 1191–1200.
34. Epple, U.; Hoffmann, F.; Schnell, M. Modeling DME interference impact on LDACS1. In Proceedings of the 2012 Integrated Communications, Navigation and Surveillance Conference, G7-1-G7-13, Herndon, VA, USA, 24–26 April 2012.
35. Brandes, S.; Schnell, M. Interference Mitigation for the Future Aeronautical Communication System in the L-Band. In *Multi-Carrier Systems & Solutions*; Plass, S., Dammann, A., Kaiser, S., Fazel, K., Eds.; Lecture Notes in Electrical Engineering; Springer: Dordrecht, The Netherlands, 2009; Volume 41.
36. Oppenheim, A.V.; Schafer, R.W. *Discrete-Time Signal Processing*; Pearson Education: London, UK, 2014.
37. Kassam, S.A. *Signal Detection in Non-Gaussian Noise*; Springer Science & Business Media: New York, NY, USA, 1988.
38. Barazideh, R.; Natarajan, B.; Nikitin, A.V.; Niknam, S.T. Performance Analysis of Analog Intermittently Nonlinear Filter in the Presence of Impulsive Noise. *IEEE Trans. Veh. Technol.* **2019**, *68*, 3565–3573. [CrossRef]
39. Blackard, K.L.; Rappaport, T.S.; Bostian, C.W.T. Measurements and models of radio frequency impulsive noise for indoor wireless communications. *IEEE J. Sel. Areas Commun.* **1993**, *10*, 991–1001. [CrossRef]
40. Sanchez, M.G.; De Haro, L.; Ramón, M.C.; Mansilla, A.; Ortega, C.M.; Oliver, D.T. Impulsive noise measurements and characterization in a UHF digital TV channel. *IEEE Trans. Electromagn. Compat.* **1999**, *41*, 124–136. [CrossRef]
41. Nakai, T.; Kawasaki, Z.T.T. On impulsive noise from Shinkansen. *IEEE Trans. Electromagn. Compat.* **1983**, *4*, 396–404. [CrossRef]
42. Dempster, A.P.; Laird, N.M.; Rubin, D.B.T. Maximum likelihood from incomplete data via the EM algorithm. *J. R. Stat. Soc. Ser. B Methodological* **1977**, *39*, 1–22.
43. Al-Naffouri, T.Y.; Quadeer, A.A.; Caire, G.T. Impulse noise estimation and removal for OFDM systems. *IEEE Trans. Commun.* **2014**, *62*, 976–989. [CrossRef]